

CERN-EP-2026-030

11 Feb 2026

Deuteron coalescence probability in jets in p–Pb collisions at $\sqrt{s_{\text{NN}}} = 5.02$ TeV

ALICE Collaboration*

Abstract

This article presents the first measurement of the (anti)deuteron and antiproton transverse-momentum distributions, the deuteron coalescence parameter, and the ratio between the yields of deuteron and proton in and out of jets in p–Pb collisions at $\sqrt{s_{\text{NN}}} = 5.02$ TeV. Three regions are used to study the jet-correlated production: Toward, Away, and Transverse to the jet axis, which direction is approximated by the leading particle in the event with $p_{\text{T}}^{\text{lead}} > 5$ GeV/ c . The jet contribution is obtained from the Toward region by subtracting the underlying event, which dominates the Transverse region. In p–Pb collisions, an enhancement of the coalescence parameter B_2 is observed in jets compared to the underlying event. The enhancement is larger than the one observed in a similar analysis already in pp collisions. The results are compared with predictions from PYTHIA 8.314 using the Angantyr model with a deuteron production model based on ordinary nuclear reactions. The model is able to qualitatively reproduce the large enhancement of the coalescence parameter in jets with respect to the out-of-jets one. The results are further compared in detail with similar ones from previous studies for pp collisions at $\sqrt{s} = 13$ TeV.

1 Introduction

The production of light (anti)nuclei has been extensively studied at different collision energies, ranging from AGS [1–4], to the SPS [5], RHIC [6–11] and the LHC [12–30]. Despite the abundance of experimental results, the production mechanism of light (anti)nuclei is still unclear. The experimental data are typically described by two different models: the statistical hadronization model (SHM) and the baryon coalescence model. In the SHM [31–38], hadrons are emitted by a source in local thermal and hadrochemical equilibrium, with the species abundance fixed at chemical freeze-out. In nucleus-nucleus collisions, given that the quantum numbers are conserved on average in all the system, the predicted hadron yields are described using the grand canonical ensemble [35], while in proton-proton and proton-nucleus collisions, since the exact conservation of the quantum numbers is required only in the correlation volume (V_C), the canonical approach is used [38]. In the coalescence model [39–46] nuclei are formed from the coalescence of protons and neutrons that are close in phase space. In a simpler approach [40] only the momentum correlations are considered, while in more advanced implementations [41, 46] the coalescence probability is calculated considering the overlap of the wave function of the individual baryons and the Wigner function of the bound state. Despite the use of the two different models, it is important to note that they do not necessarily exclude each other. In fact, the SHM only predicts the overall particle yields, not the momentum distributions. Moreover, the SHM is a macroscopic model, hence a microscopic description on the hadron formation mechanism is not discussed. The baryon coalescence model, instead, provides such microscopic description in its formulation.

Another interesting field of application concerning the study of light (anti)nuclei produced at colliders is related to indirect dark-matter searches. In fact, different space-based experiments, such as AMS-02 [47] and GAPS [48], are actively searching the signal originating from light antinuclei in cosmic rays [49–51]. In particular, the detected flux of such particles must be correctly evaluated, in order to understand their source. In the current model, antinuclei can be produced in interactions between high-energy cosmic rays and the interstellar medium, or from annihilation of dark matter. Since the former constitutes a large background for dark-matter searches, precise estimate of the antinucleus production are critical, and collider experiments can provide valuable constraints. In fact, the measurements obtained in collider experiments not only give insights in the antinucleus production mechanism, but they can also provide information on the antinucleus cross sections. Novel results from ALICE evaluate the inelastic cross section of antideuteron [52], antitriton [53], and anti³He [54] interactions with nuclei, also discussing the implications for the astrophysical searches of dark matter in the case of anti³He.

The current knowledge on the light (anti)nuclei production mechanism is still incomplete, hence innovative observables to test the models' predictions are needed. In particular, to further constrain the coalescence model, the production mechanism of light (anti)nuclei can be studied in and out of jets, as already done in Refs. [27, 55]. Jets are defined as collimated emission of hadrons produced by the hadronization of energetic quarks and gluons generated in high- Q^2 interactions. Due to the collimation, in general, hadrons in jets are closer in phase space than hadrons out of jets [56]. Hence, according to the coalescence model, an enhancement of the coalescence probability in jets is expected with respect to the same quantity out of jets, where the particles are not as strongly correlated. For this reason it is interesting to study the difference of the light (anti)nuclei production in and out of jets in small systems, such as pp and p–Pb, since the nucleons are already closer in phase space, but the two systems differ in other aspects, such as spatial dimension and multiplicity of charged particles. Specifically, the source size, i.e. the region that emits hadrons with similar momenta, that can be measured with two-particle correlation measurements through the femtoscopy method, in p–Pb is slightly larger with respect to the pp case. In this case the coalescence model predicts a smaller coalescence probability out of jets in p–Pb collisions with respect to the same quantity evaluated in pp collisions [41, 57]. For the in-jet case, instead, an enhancement of the coalescence probability with respect to the out of jet case is predicted, due to the fact that hadrons are closer in phase space. Another aspect that can be investigated is the jet hadro-

chemistry. Based on current knowledge, it should be independent of the collision system from which the jets originate [58]. Hence, similar results on particle-species compositions in jets in different collision systems are expected. If, instead, the jet hadrochemistry depends on the collision systems, differences in particle-species composition and distributions in jets could arise, with consequences on the production of light (anti)nuclei and other particles [59, 60]. In particular, for the light (anti)nuclei, the nuclei-to-proton yield ratio could give insights in the hadrochemistry.

In this article, (anti)deuteron and antiproton production is studied in and out of jets. Unlike for antiprotons, for deuterons both matter and antimatter particles are used. This choice maximizes the collected signal for the (anti)deuterons, since the production of such particles is suppressed of a factor of about 10^3 with respect to (anti)protons, while it ensures that the antiproton data sample almost exclusively consists of primary particles (except for a small fraction of secondary particles due to weak decays), since the contribution of secondary particles created in the interaction with the detector is negligible for the antimatter case. It is important to note that the results of this analysis may depend on how the jets are defined, i.e. whether a trigger particle of a given p_T or the full p_T of the jet is considered. For this reason, the same jet definition used in pp collisions is applied to allow for a comparison with the published result [27]. In each event the leading particle, that is used as a proxy for the jet axis, is defined as the particle with the highest transverse momentum, which also satisfies the condition $p_T^{\text{lead}} > 5 \text{ GeV}/c$, where p_T^{lead} is the transverse momentum of the leading particle, as reported in Ref. [61]. The transverse-momentum distributions are measured in three different azimuthal regions defined relative to the leading particle by $\Delta\phi = |\phi - \phi_{\text{lead}}|$, where ϕ is the azimuthal angle of the particle and ϕ_{lead} refers to the direction of the leading track. The obtained regions, all 120° wide, are the same as the ones defined in similar analyses [61, 62]: the region around the jet axis (Toward, $|\Delta\phi| < 60^\circ$), the region back-to-back to the jet axis (Away, $|\Delta\phi| > 120^\circ$) and the region transverse to both of them (Transverse, $60^\circ < |\Delta\phi| < 120^\circ$). The Transverse region is dominated by the underlying event, while the Toward and Away regions, in addition to the underlying event, have a contribution from the leading and recoil jet, respectively. The in-jet transverse-momentum distributions are hence obtained by subtracting the distributions in the Transverse region from the corresponding ones in the Toward region.

The coalescence parameter, which quantifies the coalescence probability [40], is defined as:

$$B_2 = \left(\frac{1}{(2\pi/3)p_T^d} \frac{1}{N_{\text{evt, trig}}} \frac{d^2 N_d}{dy dp_T^d} \right) \bigg/ \left(\frac{1}{(2\pi/3)p_T^p} \frac{1}{N_{\text{evt, trig}}} \frac{d^2 N_p}{dy dp_T^p} \right)^2, \quad (1)$$

where the labels d and p indicate the two different species, $p_T^p = p_T^d/2$, with the assumption that the neutron and proton momentum distributions are the same since they belong to the same isospin doublet, and $N_{\text{evt, trig}}$ is the number of events with a leading particle that satisfies the trigger condition. The number of events and triggers in this analysis are the same. Unlike in previous analyses [13–16, 18–21, 23, 28, 30], the (anti)deuteron and antiproton production in this analysis is studied in three regions of phase space with respect to the jet axis, which leads to an additional factor of $1/3$. This factor is the same in both the in and out of jets cases, since the two regions have the same width in ϕ $2\pi/3$.

2 ALICE detector and data samples

The ALICE apparatus is ideally suited to study light (anti)nuclei production because of its excellent tracking performance and particle-identification capabilities in a broad range of transverse momentum. A detailed description of the ALICE subsystems and their performance can be found in Refs. [63, 64] and references therein.

The detectors used in this analysis, which are briefly described below in their state during the Run 2 data taking, are the Inner Tracking System (ITS), the Time Projection Chamber (TPC), and the Time-Of-

Flight (TOF) detector. These detectors are located inside a solenoidal magnet with a field strength of $B = 0.5$ T.

The ITS [63] is used to reconstruct the primary vertex of the collision and the secondary vertices from weak decays. It covers the full azimuthal angle and the pseudorapidity interval $|\eta| < 0.9$ and is composed of six cylindrical layers of silicon detectors, with a radial distance ranging from 3.9 cm to 43 cm. Three different technologies are used: the two innermost layers are Silicon Pixel Detectors (SPD), followed by two layers of Silicon Drift Detectors (SDD), and the two outermost layers are Silicon Strip Detectors (SSD).

The TPC [65] is the main ALICE tracking detector. It is a cylindrical drift chamber with a length of 500 cm in the beam direction and a radius ranging from 85 to 250 cm, covering the same pseudorapidity interval of the ITS. The vessel is filled with a gas mixture of 90% Ar and 10% CO₂ at atmospheric pressure. The cage is closed with two endcaps made of Multi-Wire Proportional Chambers (MWPCs). The particle identification is obtained by measuring the specific energy loss (dE/dx) in the gas, while the trajectory is reconstructed using up to 159 space points reconstructed in the TPC volume.

The TOF detector [66] is formed by Multi-gap Resistive Plate Chambers (MRPCs) located at a radial distance of 380 cm from the beam axis. It measures the arrival time of charged particles relative to the event collision time provided by the TOF itself and by the T0 detector [67]. The T0 detector consists of two arrays of Cherenkov counters (T0A and T0C) placed at opposite sides of the interaction point, covering the pseudorapidity regions $4.6 < \eta < 4.9$ and $-3.3 < \eta < -3.0$.

The V0 detector [68] is used to define the minimum bias trigger, and to separate beam-beam interactions from background events such as beam-gas interactions. It is formed by two plastic scintillator arrays (V0A and V0C) placed at both sides of the interaction point and covering the pseudorapidity regions $2.8 < \eta < 5.1$ and $-3.7 < \eta < -1.7$.

A data sample collected by ALICE in 2016 during the LHC p–Pb campaign at $\sqrt{s_{NN}} = 5.02$ TeV is used in this analysis. The events are selected with a minimum bias trigger, where the signals in both V0 scintillators must be synchronous with the beam crossing time defined by the LHC clock. Events with multiple vertices identified with the SPD are tagged as pile-up and removed from the analysis. To ensure a uniform detector response, only events with a reconstructed vertex position along the beam axis within 10 cm from the nominal interaction point are considered. With these requirements, a data sample of about 310 million minimum bias events is selected. Since the energy per nucleon of the proton beam is higher with respect to the Pb beam, the midrapidity axis in the center-of-mass frame is shifted with respect to the laboratory frame by -0.465 units of rapidity in the direction of the proton beam [19], that travels toward the negative z -direction. For this reason, the rapidity of each track in the laboratory system needs to be transformed into the centre-of-mass system applying the following formula:

$$y_{\text{CMS}} = y_{\text{lab}} + 0.465. \quad (2)$$

After applying such a shift to all the particles, only the ones with $-0.07 < y_{\text{CMS}} < 0.93$ are selected. To identify events that contain a jet, only events with at least one charged primary particle with $p_{\text{T}}^{\text{lead}} > 5$ GeV/ c are considered. The final data sample corresponds to approximately 2.4% of the minimum-bias p–Pb collisions.

3 Analysis procedure

In this section the analysis procedure is reported, including the track selection criteria, particle identification and signal extraction, corrections derived from Monte Carlo (MC) simulations, and the evaluation of the systematic uncertainties.

3.1 Track selection and particle identification

Antiproton and (anti)deuteron candidates are selected among charged-particle tracks reconstructed in the ITS and TPC in the kinematic range $|\eta| < 0.8$. Reconstructed tracks are required to fulfill a set of quality criteria. The minimum number of clusters required in the ITS must be higher than two or four for the (anti)deuteron and antiproton, respectively, with at least one cluster located in one of the two innermost ITS layers in both cases. The minimum number of clusters in the TPC must be 50 for the (anti)deuteron and 60 for antiproton. To ensure accurate reconstruction of the fitted tracks, the χ^2 per degree of freedom is required to be less than four for the TPC for both species. The contribution of secondary nuclei is reduced by requiring that the distance of closest approach (DCA) to the primary vertex in the transverse plane (DCA_{xy}) and longitudinal direction (DCA_z) is lower than, respectively, 0.1 and 1.0 cm for both species. The leading particle is defined as the track with the highest transverse momentum among those fulfilling the same quality criteria used in previous analyses [27, 61, 62].

In the three azimuthal regions, the same procedure for signal extraction is applied. Antiprotons with $0.3 < p_T < 0.7$ GeV/c and (anti)deuterons with $0.6 < p_T < 1.2$ GeV/c are identified by requiring that the specific energy loss dE/dx measured by the TPC [65] is within 3σ of the expected value predicted by the Bethe-Bloch parametrization. For (anti)deuterons between $1.0 < p_T < 1.2$ GeV/c, the contamination from (anti)protons is fitted with a Gaussian function and subtracted. At higher transverse momenta, i.e. $0.7 < p_T < 1.5$ GeV/c for antiprotons and $1.2 < p_T < 3.0$ GeV/c for (anti)deuterons, the particle identification is performed using the TPC and TOF detectors, where the TOF time-of-flight distributions [66] are analyzed for the particles that satisfied the TPC pre-selection criteria, $|n\sigma_{\text{TPC}}| < 3$, defined as $n\sigma_{\text{TPC}} = (dE/dx - \langle dE/dx \rangle_i) / \sigma_{\text{TPC},i}$, where dE/dx is the measured signal in the TPC, $\langle dE/dx \rangle_i$ is the expected signal for the particle species i and $\sigma_{\text{TPC},i}$ is the detector resolution for that species. The signal is extracted from a fit of the $n\sigma_{\text{TOF}} = (\Delta t - \Delta t_i) / \sigma_{\text{TOF},i}$ distribution, where Δt is the measured time-of-flight, Δt_i is the expected value for the different species, and $\sigma_{\text{TOF},i}$ is the detector resolution for the considered species. The distribution is fitted with an exponentially modified Gaussian function with a tail on the right, while the background derived from mismatched tracks is parameterized with a single or double exponential (depending on the p_T interval) for the (anti)deuterons or with a second-order polynomial for the antiprotons. The signal extraction is performed by integrating the distribution in the interval $[\mu_0 - 3\sigma_{\text{TOF}}, \mu_0 + 3.5\sigma_{\text{TOF}}]$, where μ_0 is the mean of the Gaussian signal, which corrects for small miscalibration effects in the TOF that have been observed in a previous analyses [12, 27, 28]. The asymmetric integration interval is chosen to take into account the exponential tail of the distribution, mainly due to tracks inducing signals in more than one detector readout element.

3.2 Corrections

The obtained raw distributions are corrected for the reconstruction efficiency and the secondary-particle contribution using MC simulated events. In particular, for the reconstruction efficiency, a MC simulation with light (anti)nuclei generated with a flat p_T distribution in the transverse-momentum range $0 < p_T < 10$ GeV/c and a flat rapidity distribution in the range $-1 < y_{\text{CMS}} < 1$ is used. The generated particles are injected on top of the underlying event generated by HIJING [69]. The interactions of the generated particles with the experimental apparatus are modeled with the Geant4 package [70]. For the secondary particles evaluation, instead, a MC simulation where the particle production is described by DPMJET [71] is used.

3.2.1 Efficiency and acceptance

The Acceptance \times Efficiency ($A \times \epsilon$) correction is calculated as the ratio of reconstructed and generated (anti)nuclei momentum distributions in the simulation, with the same track selections as used for the data applied in the reconstructed MC. The obtained efficiency for (anti)deuterons ranges from 45 to 80% in the p_T interval $0.6 < p_T < 1.2$ GeV/c, where only the information from the TPC is used. It is about 50%

Table 1: Summary of the different contributions of the systematic uncertainties, both for (anti)deuterons and antiprotons, in the lowest and highest p_T intervals. All values are given as percentages.

Particle p_T range (GeV/c)	d (\bar{d})		\bar{p}		
	0.6 – 0.8	2.4 – 3.0	0.3 – 0.4	1.4 – 1.5	
Source of uncertainty					
Tracking	0.3 (1.5)	0.5 (0.9)	0.7	2.4	
ITS-TPC matching	1.0 (1.0)	1.0 (1.0)	1.0	1.0	
Material budget	1.0 (1.0)	1.0 (1.0)	1.0	1.0	
Hadronic interaction	0.4 (3.0)	0.7 (4.0)	0.3	1.4	
Primary fraction	5.0 (-)	negl. (-)	1.0	1.1	
Signal extraction	Toward	1.4 (1.0)	1.8 (2.6)	0.7	0.5
	Transverse	1.4 (1.9)	3.7 (2.8)	0.6	0.5
	Away	2.1 (1.5)	2.8 (2.1)	0.7	0.6

in the remaining transverse-momentum range, where the particle identification is complemented with the TOF information. Moreover, in all transverse-momentum ranges, the efficiency for antideuterons is smaller than that for deuterons, due to the annihilation processes with the detector material. For antiprotons the obtained values are between 25 and 65% for transverse momentum below 0.7 GeV/c, while for $0.7 < p_T < 1.5$ GeV/c the efficiency ranges from 30 to 40%.

3.2.2 Secondary particles from spallation and weak decays

Primary particles can interact with the detector material and produce nuclear fragments, called spallation products. Since antinuclei cannot originate from the detector material, this contamination only applies to deuterons. The fraction of secondary nuclei from the material is obtained from template fits to the measured DCA_{xy} distributions, as done in previous measurements [18, 20] and described in Ref. [13]. Antideuterons from data are used as a template for primary deuterons, while the template for secondary deuterons from spallation is taken from MC simulations. The fit is executed in the range $|DCA_{xy}| < 1.0$ cm. The obtained fraction of secondary deuterons varies from 45% in the lowest p_T range, and approaches zero for $p_T > 1.8$ GeV/c.

For antiprotons the secondary contamination arises from weak decays of strange particles, such as Λ and Σ baryons. A procedure similar to that used for deuterons is applied to antiprotons, although in this case both the primary and secondary templates are obtained using MC simulations. The fit is performed in the same DCA_{xy} intervals, and the secondary fraction, of about 20%, is found to be weakly dependent on p_T .

3.3 Systematic uncertainties

The different contributions to the systematic uncertainties of (anti)deuterons and antiprotons are reported in Tab. 1. The final value is obtained as the sum in quadrature of all contributions, and it varies from 3 to 5% for (anti)deuterons and is about 3% for antiprotons.

For the systematic uncertainty of the track reconstruction, the quality criteria used in the analysis and reported in Sect. 3.1 are varied 50 times both in data and MC simulations using a random uniform distribution around each nominal value. The width of the variation differs for the individual quality criteria as sources of uncertainty, while maintaining a good overall quality of the reconstructed tracks. The relative systematic uncertainty is given by the standard deviation over the mean value of the distribution of the selected particles, considering the corrected yield for each transverse-momentum interval. This contribution is between 0.3% (1.5%) and 0.5% (0.9%) for deuterons (antideuterons), while it varies from 0.7 to 2.4% for antiprotons. At low p_T , the uncertainty for antideuterons is larger than for deuterons, due to

statistical fluctuations in the applied procedure.

The uncertainty due to the ITS-TPC matching efficiency is evaluated as the difference between data and MC. The obtained value, of about 1% for both species, is p_T independent.

The systematic uncertainty due to material budget, equal to 1% for both (anti)deuterons and antiprotons, is taken from Ref. [20]. This source is estimated by comparing different MC simulations in which the material budget is increased and decreased by 4.5%, which is the uncertainty in determining the material budget of the detector [64].

The uncertainty due to the hadronic interaction cross section with the detector material is estimated by varying the default inelastic cross section of the selected species in Geant4 within its uncertainty, obtained with measurements on different targets [72–80]. The obtained value is p_T dependent, since at high transverse momentum the particle identification is obtained using different detectors, hence different hadronic processes may contribute. Moreover, matter and antimatter are subjected to different hadronic interactions with the detector material, with different cross section values. For this reason, this systematic uncertainty for deuteron and antideuteron has different values. The obtained uncertainty varies from 0.4% (3.0%) to 0.7% (4.0%) for deuterons (antideuterons), while for antiprotons it rises from 0.3% at low p_T to 1.4% at high p_T .

The systematic uncertainty on the primary fraction is obtained by varying the longitudinal and transverse DCA selection criteria, the intervals width, and the fit interval for the template method. The obtained value for each case is equal to the difference between the highest and lowest values divided by two. This source of systematic uncertainty is negligible for antideuterons (due to the fact that antinuclei are not produced by spallation processes), while it is relevant for deuterons at low transverse momentum, where it reaches 5%. The same contribution for the antiproton is weakly dependent on p_T and equals about 1%.

Finally, the systematic uncertainty due to the signal extraction, calculated for the three azimuthal regions due to the azimuthal dependence of the signal extraction procedure in the analysis, is evaluated with different methods. These include varying the integration interval (considering 50 variations of the integration interval where the extremes are uniformly generated in the range $[-3.5n\sigma_{\text{TPC}}, -2.0n\sigma_{\text{TPC}}]$ and $[2.0n\sigma_{\text{TPC}}, 3.5n\sigma_{\text{TPC}}]$ for the TPC, and $[-3.0n\sigma_{\text{TOF}}, -2.0n\sigma_{\text{TOF}}]$ and $[3.0n\sigma_{\text{TOF}}, 4.5n\sigma_{\text{TOF}}]$ for the TOF), using a different parametrization for the background functions (like Gaussian or exponential function for the TPC), and varying the signal extraction strategy (considering bin counting or the integral of the signal function). For the former, the obtained value is equal to the ratio between the standard deviation and the mean of the distribution of the corrected yield, where the efficiency is also calculated considering the different integration intervals. For the others, half of the difference between the obtained value and the nominal value is considered. This source is different in the three azimuthal regions, ranging from a minimum of 1.4% to a maximum of 3.7% for (anti)deuterons, while for antiprotons it ranges between 0.5% and 0.7%.

4 Results

The p_T distributions of the average of deuteron and antideuteron in the three azimuthal regions are shown in Fig. 1 (top-left) while the distributions for antiprotons are displayed in the bottom left panel. The dotted lines represent Lévy-Tsallis fits [81]. For the mean of deuteron and antideuteron, the total systematic uncertainty is propagated considering the two errors to be independent. The distributions in the different regions are scaled for visibility reasons. For both species, the transverse-momentum distributions in the Toward and Away regions are compatible, while the Transverse is about 90% of the Toward region. These experimental results are consistent with the one already observed in pp collisions [27]. The in-jet transverse-momentum distribution is obtained by subtracting the distribution in the Transverse region (which is dominated by the underlying event) from the distribution in the Toward region (which contains

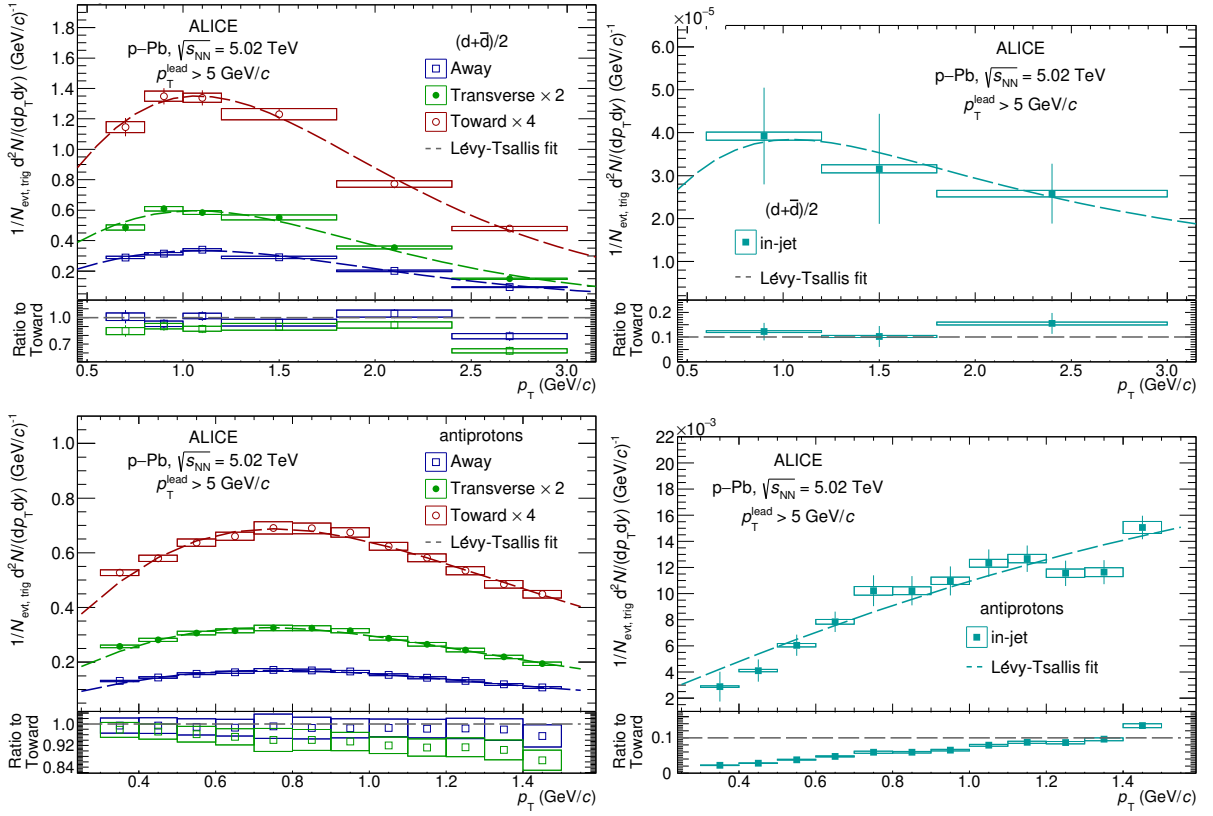


Figure 1: The average of deuteron and antideuteron (top row) and antiproton (bottom row) p_T -differential yields in the three azimuthal regions (left) and in jets (right) measured in p-Pb collisions at $\sqrt{s_{\text{NN}}} = 5.02$ TeV. Statistical and systematic uncertainties are reported, respectively, with vertical lines and boxes. Individual Lévy-Tsallis fits are also shown. The distributions are scaled for visibility reasons. The bottom panel of each figure shows the ratio of the distribution with respect to the Toward one.

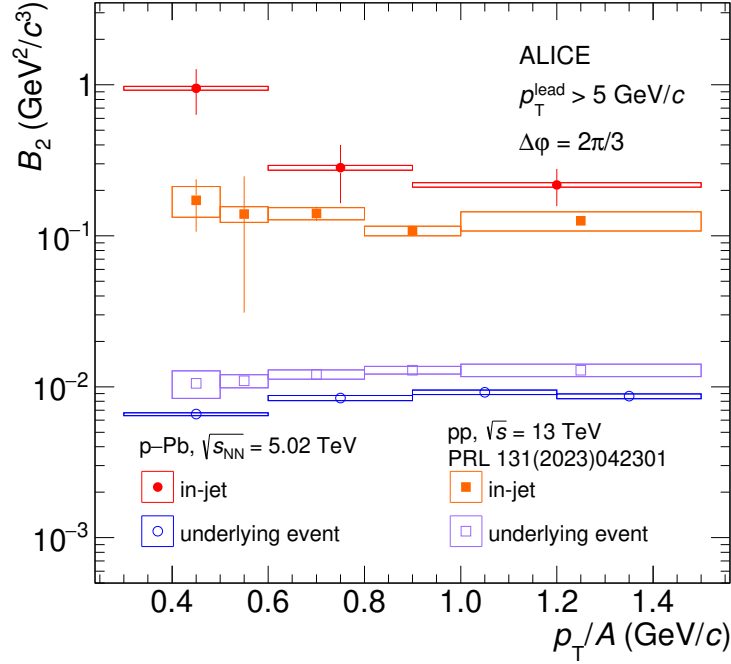


Figure 2: The coalescence parameter in jets B_2^{jet} and in the underlying event B_2^{UE} as a function of the per nucleon transverse momentum p_T/A (here, $A = 2$) in pp collisions at $\sqrt{s} = 13$ TeV, taken from [27], and p–Pb collisions at $\sqrt{s_{\text{NN}}} = 5.02$ TeV. Statistical and systematic uncertainties are represented, respectively, by vertical bars and boxes.

both jet fragmentation and underlying event). These distributions for both the average between deuteron and antideuteron and antiproton are reported in Fig. 1 (right). In the case of the mean of the deuteron and antideuteron, due to the reduced data sample available, the TPC transverse-momentum intervals and the two last TOF p_T intervals have been merged using a weighted mean, using as weight the value of the Lévy-Tsallis function. The total systematic uncertainty for the mean of deuteron and antideuteron in-jet spectrum is calculated considering the mean of the sum in quadrature of the systematic uncertainty of the two particle species. For each species, the total in-jet systematic uncertainty is equal to the sum in quadrature of the contribution listed in Tab. 1, where the signal extraction one is calculated as the sum in quadrature of the Toward and Transverse regions. A similar approach has been applied to the antiproton in-jet spectrum. As already observed in pp collisions [22, 27], the jet contribution accounts only for about 10% of the total particle production in the Toward region. Hence, with the jet reconstruction adopted in this analysis, also the Toward region is dominated by the underlying event. Moreover, as expected in the case of the jet-associated particle production [82], the distributions in jets show a hardening with respect to the one out of jets. It is worth to notice that these distributions can be influenced by the long range correlations and the different elliptic flow of the (anti)deuterons and antiprotons.

With the obtained distributions, the coalescence parameter in jets (B_2^{jet}) and in the underlying event (B_2^{UE}) is calculated according to Eq. 1. This quantity is shown in Fig. 2 as a function of the per-nucleon transverse momentum, p_T/A , where $A = 2$ is the mass number of the deuteron. The figure shows both B_2^{jet} (full markers) and B_2^{UE} (empty markers) in pp collisions at $\sqrt{s} = 13$ TeV (square markers), taken from [27], and in p–Pb collisions at $\sqrt{s_{\text{NN}}} = 5.02$ TeV (circle markers). The coalescence parameter B_2^{jet} is enhanced with respect to B_2^{UE} in p–Pb collisions by more than a factor of 20 with a significance of about 4.6σ , larger than the enhancement of about 15, observed in pp collisions [27]. One explanation provided by the coalescence model for this enhancement is the reduced distance in phase space between nucleons in jets compared with the underlying event.

More information can be obtained if the values observed in the two collision systems are compared in

the single azimuthal regions. In particular, in the underlying event region, the B_2^{UE} in p–Pb collisions is lower with respect to the same quantity in pp collisions. This can be explained by considering the dependence of the coalescence parameter on the source size. According to the coalescence model [41], the coalescence parameter decreases with increasing source size, since the nucleons are naturally more spread out in phase space. The source size of the pp and p–Pb colliding systems, in particular the values of the source radii, have been measured by ALICE through femtoscopy techniques [83]. The obtained values are of about 1 fm in pp collisions [84] and 1.5 fm in p–Pb collisions [85].

The different values of the coalescence parameter in jets, where the p–Pb values are larger than in pp collisions, do not have a unique explanation at the moment. They could arise from different particle-species composition of jets in the two systems, stronger momentum correlation between the nucleons, or a higher average p_T value in jets. Moreover, a dependence on p_T/A is observed. In order to distinguish among these different explanations, specific analyses that investigate these hypotheses and a larger data sample might be considered, since the in-jet results are dominated by the statistical uncertainty.

The obtained results are compared with the predictions from a reaction-based deuteron production model implemented in PYTHIA 8.314 [86] with the Angantyr model [87]. Angantyr, inspired by the Fritiof model [88, 89], uses the Glauber model to calculate the number of wounded nucleons and generate the hadronic final state in proton-nucleus and nucleus-nucleus collisions. Deuteron production is implemented in PYTHIA 8.314 with a nuclear reactions-based model reported in detail in Refs. [27, 86]. Only statistical uncertainties are computed in the model. As shown in Fig. 3, the model qualitatively reproduces the data, as already observed in pp collisions [27]. In particular, the model is able to reproduce the enhancement of B_2^{jet} with respect to B_2^{UE} . While the predictions for B_2^{UE} are consistent with the experimental data, the B_2^{jet} seems to be underestimated by the model at low p_T/A values, though the current statistical uncertainties do not allow a conclusive statement. The comparison with such a model, even if a state-of-the-art coalescence approach is not implemented, gives significant insights in the deuteron production, considering the recent results reported in Ref. [90]. In such study, in fact, the deuteron-pion correlation function shows that the deuteron is produced through nuclear fusion processes, and PYTHIA 8.314 uses a similar approach for the deuteron production.

The ratio of the measured yields of deuterons and protons is also sensitive to the production mechanism of light nuclei. In particular, this ratio can give more insights in hadrochemistry, exploring the differences across different collision systems. The deuteron-to-proton yield ratio as a function of the reduced transverse momentum p_T/A is reported in the top row of Fig. 4 for both pp collisions at $\sqrt{s} = 13$ TeV (left panels) and p–Pb collisions at $\sqrt{s_{\text{NN}}} = 5.02$ TeV (right panels) both in the jet region (red, full marker) and in the underlying event (blue, open marker). The deuteron and proton distributions in the pp case are taken, respectively, from Refs. [27, 91]. In the ratio, the statistical uncertainties are treated as independent. In both collision systems, the ratio of deuterons to protons is higher in jets with respect to the underlying event, as reported in the bottom row in Fig. 4, by a factor between one and two in pp collisions and between two and four in p–Pb collisions. These results suggest that the deuteron production is favored in jets with respect to the production out of jets, which could be explained by considering the enhanced coalescence probability in jets.

A further comparison is made by considering the ratio of the deuteron to proton ratios of the two collision systems in the different azimuthal regions. This comparison is reported in Fig. 5. In this case, since the p_T intervals of the two analyses are not the same, an interpolation of the experimental points is used to evaluate the ratio. The systematic uncertainties are treated as independent when propagating them through the double ratio. Finally, the uncertainty of the double ratio is equal to the quadrature sum of the statistical and systematic uncertainties. For the in-jet region the statistical uncertainty dominates, being about 90% of the total error. For the underlying event region, in contrast, statistical and systematic uncertainties are comparable in each interval of p_T/A . The results, reported in the bottom row of Fig. 5, show that in both jets and the underlying event the double ratio is compatible with unity within the

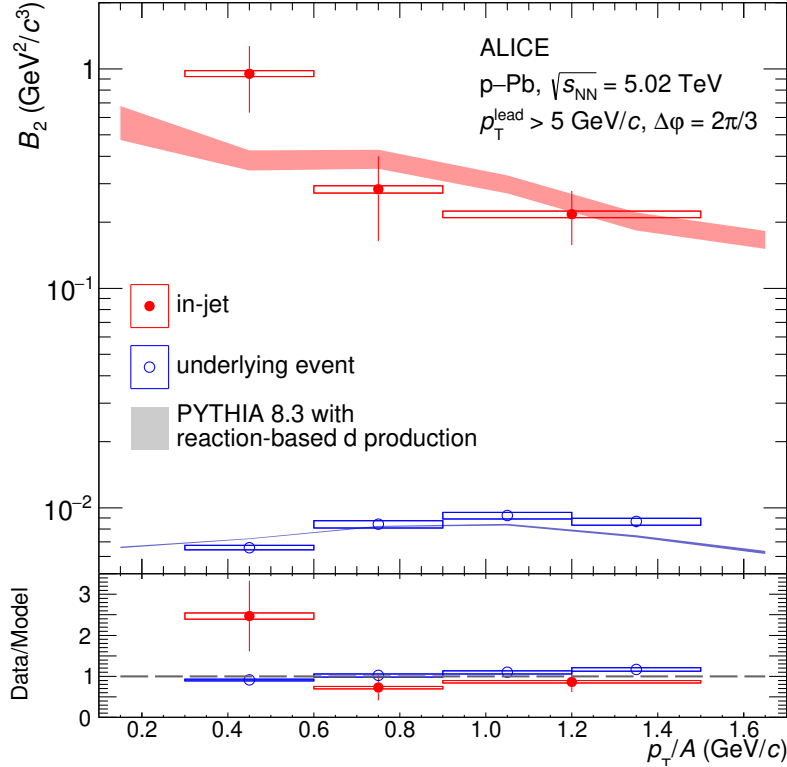


Figure 3: The coalescence parameter in jets B_2^{jet} and in the underlying event B_2^{UE} in p–Pb collisions at $\sqrt{s_{\text{NN}}} = 5.02$ TeV as a function of p_{T}/A compared with the model prediction given by PYTHIA 8.314 with Angantyr.

1σ uncertainty, and therefore no firm conclusion on the jet hadrochemistry in different systems can be drawn. To fully address the observed results further detailed studies of jet hadrochemistry are required, as the present results do not allow a definitive statement due to the limited jet-spectra data sample and the dominance of statistical uncertainties in the analysis.

5 Summary and conclusions

This article presents the measurement of (anti)deuteron and antiproton distributions, and the deuteron coalescence parameter in and out of jets in p–Pb collisions at $\sqrt{s_{\text{NN}}} = 5.02$ TeV, complementing and extending the study presented in Ref. [27] for pp collisions. This experimental observation is consistent with the coalescence picture that predicts an enhanced formation probability of a bound state for nucleons that have a small average phase-space distance. The results are compared with previous measurements from pp collisions at $\sqrt{s} = 13$ TeV. The enhancement of B_2^{jet} with respect to B_2^{UE} measured in p–Pb collisions, a factor more than 20 with a 4.6σ significance, is larger with respect to the one observed in pp collisions, of about 15. Such a result could be explained by the different source sizes and, possibly, by different particle-species compositions of jets in the two collision systems. Moreover, the deuteron-to-proton ratio is enhanced in jets with respect to the underlying event in both pp and p–Pb collisions by a factor between one and two in the pp case and between two and four in p–Pb collisions. Comparing the d/p values in jets and in the underlying event between the two different collision systems, their ratio is compatible with unity within the 1σ uncertainty, hence no firm conclusion on the jet hadrochemistry in different systems can be drawn. The obtained results on the coalescence parameter are compared with the predictions from PYTHIA 8.314 with the Angantyr model, which is able to qualitatively reproduce the large gap in the observable, even if B_2^{jet} seems to be underestimated by the model at low p_{T}/A . However, the current statistical uncertainties do not allow for a conclusive statement.

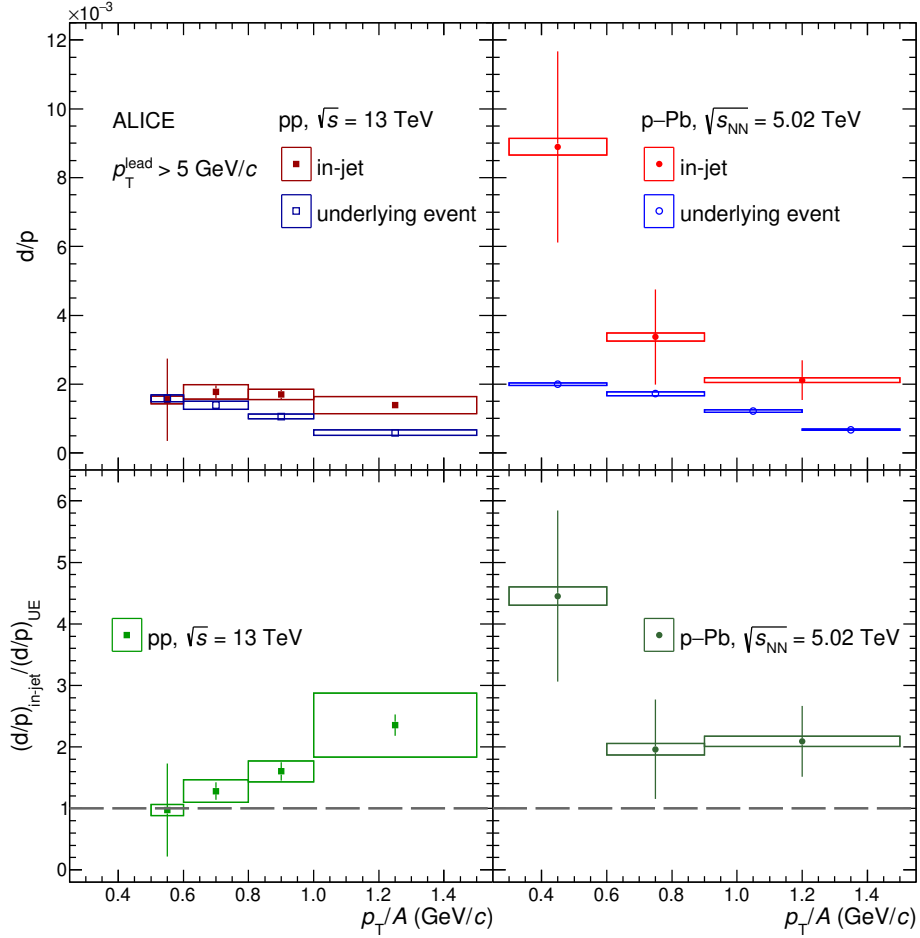


Figure 4: Top: The deuteron-to-proton yield ratio in pp collisions at $\sqrt{s} = 13$ TeV [27, 91] (left) and p-Pb collisions at $\sqrt{s_{\text{NN}}} = 5.02$ TeV (right) in jets and in the underlying event. Bottom: The double ratio $(d/p)_{\text{in-jet}}/(d/p)_{\text{UE}}$ in pp collisions at $\sqrt{s} = 13$ TeV (left) and p-Pb collisions at $\sqrt{s_{\text{NN}}} = 5.02$ TeV (right). Statistical and systematic uncertainties are represented, respectively, by vertical bars and boxes.

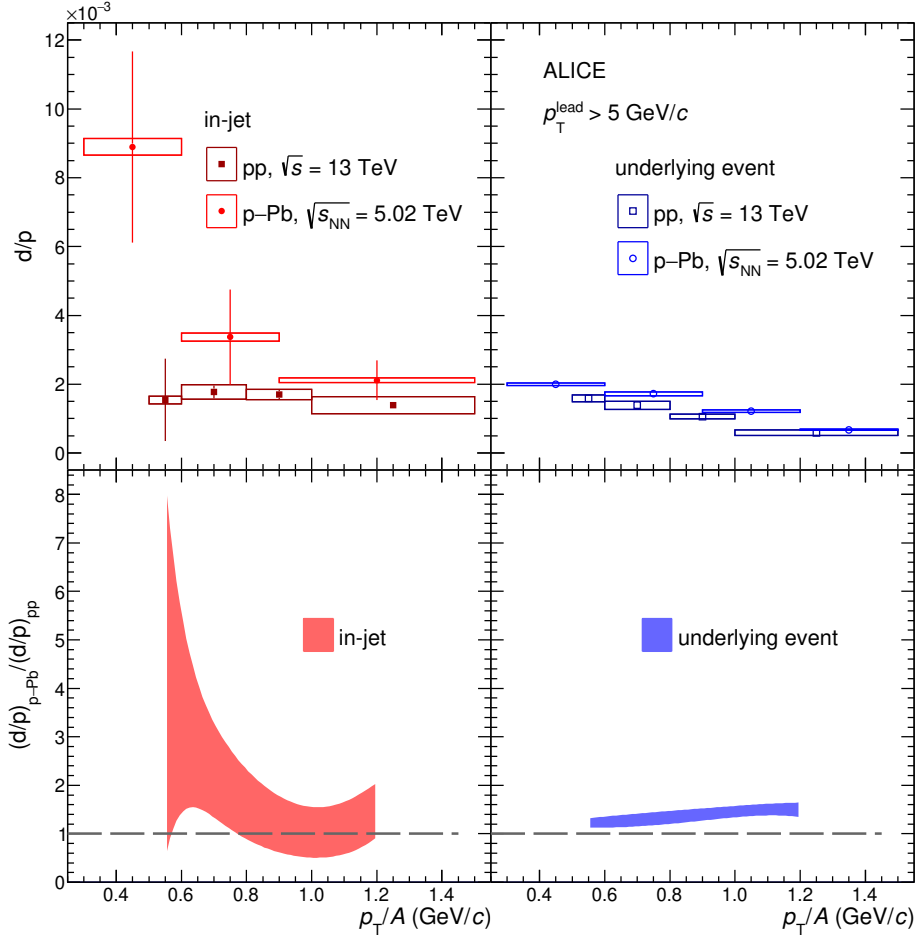


Figure 5: Top: The deuteron-to-proton yield ratio in jets (left) and in the underlying event (right) in pp collisions at $\sqrt{s} = 13 \text{ TeV}$ [27, 91] and p-Pb collisions at $\sqrt{s_{NN}} = 5.02 \text{ TeV}$ (right). Statistical and systematic uncertainties are represented, respectively, by vertical bars and boxes. Bottom: The double ratio $(d/p)_{p\text{-Pb}}/(d/p)_{pp}$ in jets (left) and in the underlying event (right). The band represents the statistical and systematic uncertainties summed in quadrature.

Future studies exploiting the larger data sample from LHC Run 3 will be extended to heavier (anti)nuclei, such as (anti)³He, applying a multi-differential approach by varying the p_T^{lead} selection, considering different transverse particle multiplicity, and fully reconstructing jets with a jet-finder algorithm. Further investigations of the coalescence parameter in and out of jets will provide additional information to constrain the light (anti)nuclei formation process, which could be used as input for further experimental measurements of the production of nuclei in colliders and in space-based experiments.

Acknowledgements

The ALICE Collaboration would like to thank all its engineers and technicians for their invaluable contributions to the construction of the experiment and the CERN accelerator teams for the outstanding performance of the LHC complex. The ALICE Collaboration gratefully acknowledges the resources and support provided by all Grid centres and the Worldwide LHC Computing Grid (WLCG) collaboration. The ALICE Collaboration acknowledges the following funding agencies for their support in building and running the ALICE detector: A. I. Alikhanyan National Science Laboratory (Yerevan Physics Institute) Foundation (ANSL), State Committee of Science and World Federation of Scientists (WFS), Armenia; Austrian Academy of Sciences, Austrian Science Fund (FWF): [M 2467-N36] and Nationalstiftung für Forschung, Technologie und Entwicklung, Austria; Ministry of Communications and High Technologies, National Nuclear Research Center, Azerbaijan; Rede Nacional de Física de Altas Energias (Renafae), Financiadora de Estudos e Projetos (Finep), Fundação de Amparo à Pesquisa do Estado de São Paulo (FAPESP) and The Sao Paulo Research Foundation (FAPESP), Brazil; Bulgarian Ministry of Education and Science, within the National Roadmap for Research Infrastructures 2020-2027 (object CERN), Bulgaria; Ministry of Education of China (MOEC), Ministry of Science & Technology of China (MSTC) and National Natural Science Foundation of China (NSFC), China; Ministry of Science and Education and Croatian Science Foundation, Croatia; Centro de Aplicaciones Tecnológicas y Desarrollo Nuclear (CEADEN), Cubaenergía, Cuba; Ministry of Education, Youth and Sports of the Czech Republic, Czech Republic; The Danish Council for Independent Research | Natural Sciences, the VILLUM FONDEN and Danish National Research Foundation (DNRF), Denmark; Helsinki Institute of Physics (HIP), Finland; Commissariat à l’Energie Atomique (CEA) and Institut National de Physique Nucléaire et de Physique des Particules (IN2P3) and Centre National de la Recherche Scientifique (CNRS), France; Bundesministerium für Forschung, Technologie und Raumfahrt (BMFTR) and GSI Helmholtzzentrum für Schwerionenforschung GmbH, Germany; National Research, Development and Innovation Office, Hungary; Department of Atomic Energy Government of India (DAE), Department of Science and Technology, Government of India (DST), University Grants Commission, Government of India (UGC) and Council of Scientific and Industrial Research (CSIR), India; National Research and Innovation Agency - BRIN, Indonesia; Istituto Nazionale di Fisica Nucleare (INFN), Italy; Japanese Ministry of Education, Culture, Sports, Science and Technology (MEXT) and Japan Society for the Promotion of Science (JSPS) KAKENHI, Japan; Consejo Nacional de Ciencia (CONACYT) y Tecnología, through Fondo de Cooperación Internacional en Ciencia y Tecnología (FONCICYT) and Dirección General de Asuntos del Personal Académico (DGAPA), Mexico; Nederlandse Organisatie voor Wetenschappelijk Onderzoek (NWO), Netherlands; The Research Council of Norway, Norway; Pontificia Universidad Católica del Perú, Peru; Ministry of Science and Higher Education, National Science Centre and WUT ID-UB, Poland; Korea Institute of Science and Technology Information and National Research Foundation of Korea (NRF), Republic of Korea; Ministry of Education and Scientific Research, Institute of Atomic Physics, Ministry of Research and Innovation and Institute of Atomic Physics and Universitatea Nationala de Stiinta si Tehnologie Politehnica Bucuresti, Romania; Ministerstvo školstva, vyzkumu, vyvoja a mladeze SR, Slovakia; National Research Foundation of South Africa, South Africa; Swedish Research Council (VR) and Knut & Alice Wallenberg Foundation (KAW), Sweden; European Organization for Nuclear Research, Switzerland; Suranaree University of Technology (SUT), National Science and Technology Development Agency (NSTDA) and National Science, Research and Innovation Fund (NSRF

via PMU-B B05F650021), Thailand; Turkish Energy, Nuclear and Mineral Research Agency (TEN-MAK), Turkey; National Academy of Sciences of Ukraine, Ukraine; Science and Technology Facilities Council (STFC), United Kingdom; National Science Foundation of the United States of America (NSF) and United States Department of Energy, Office of Nuclear Physics (DOE NP), United States of America. In addition, individual groups or members have received support from: FORTE project, reg. no. CZ.02.01.01/00/22_008/0004632, Czech Republic, co-funded by the European Union, Czech Republic; European Research Council (grant no. 950692), European Union; Deutsche Forschungs Gemeinschaft (DFG, German Research Foundation) “Neutrinos and Dark Matter in Astro- and Particle Physics” (grant no. SFB 1258), Germany; FAIR - Future Artificial Intelligence Research, funded by the NextGenerationEU program (Italy).

References

- [1] **E878** Collaboration, M. J. Bennett *et al.*, “Light nuclei production in relativistic Au + nucleus collisions”, *Phys. Rev. C* **58** (1998) 1155–1164.
- [2] **E802** Collaboration, L. Ahle *et al.*, “Proton and deuteron production in Au+Au reactions at 11.6A GeV/c”, *Phys. Rev. C* **60** (Oct, 1999) 064901.
- [3] **E864** Collaboration, T. A. Armstrong *et al.*, “Measurements of light nuclei production in 11.5A GeV/c Au+Pb heavy-ion collisions”, *Phys. Rev. C* **61** (May, 2000) 064908.
- [4] **E864** Collaboration, T. A. Armstrong *et al.*, “Antideuteron Yield at the AGS and Coalescence Implications”, *Phys. Rev. Lett.* **85** (2000) 2685–2688.
- [5] **NA52 (Newmass)** Collaboration, G. Ambrosini *et al.*, “Baryon and antibaryon production in lead-lead collisions at 158AGeV/c”, *Phys. Lett. B* **417** (1998) 202–210.
- [6] **STAR** Collaboration, C. Adler *et al.*, “Measurement of Inclusive Antiprotons from Au+Au Collisions at $\sqrt{s_{NN}} = 130$ GeV”, *Phys. Rev. Lett.* **87** (2001) 262302.
- [7] **PHENIX** Collaboration, S. S. Adler *et al.*, “Deuteron and Antideuteron Production in Au + Au Collisions at $\sqrt{s_{NN}} = 200$ GeV”, *Phys. Rev. Lett.* **94** (2005) 122302.
- [8] **BRAHMS** Collaboration, I. Arsene *et al.*, “Rapidity dependence of deuteron production in central Au + Au collisions at $\sqrt{s_{NN}} = 200$ GeV”, *Phys. Rev. C* **83** (2011) 044906, arXiv:1005.5427 [nucl-ex].
- [9] **STAR** Collaboration, H. Agakishiev *et al.*, “Observation of the antimatter helium-4 nucleus”, *Nature* **473** (2011) 353–356, arXiv:1103.3312 [nucl-ex]. Erratum: *Nature* 475 (2011) 412.
- [10] **STAR** Collaboration, L. Adamczyk *et al.*, “Measurement of elliptic flow of light nuclei at $\sqrt{s_{NN}} = 200, 62.4, 39, 27, 19.6, 11.5, \text{ and } 7.7$ GeV at the BNL Relativistic Heavy Ion Collider”, *Phys. Rev. C* **94** (2016) 034908, arXiv:1601.07052 [nucl-ex].
- [11] **STAR** Collaboration, J. Adam *et al.*, “Beam energy dependence of (anti-)deuteron production in Au + Au collisions at the BNL Relativistic Heavy Ion Collider”, *Phys. Rev. C* **99** (2019) 064905, arXiv:1903.11778 [nucl-ex].
- [12] **ALICE** Collaboration, J. Adam *et al.*, “Precision measurement of the mass difference between light nuclei and anti-nuclei”, *Nature Physics* **11** (2015) 811–814, arXiv:1508.03986 [nucl-ex].

- [13] ALICE Collaboration, J. Adam *et al.*, “Production of light nuclei and anti-nuclei in pp and Pb-Pb collisions at energies available at the CERN Large Hadron Collider”, *Phys. Rev. C* **93** (2016) 024917, arXiv:1506.08951 [nucl-ex].
- [14] ALICE Collaboration, S. Acharya *et al.*, “Multiplicity dependence of (anti-)deuteron production in pp collisions at $\sqrt{s} = 7$ TeV”, *Phys. Lett. B* **794** (2019) 50–63, arXiv:1902.09290 [nucl-ex].
- [15] ALICE Collaboration, S. Acharya *et al.*, “Measurement of deuteron spectra and elliptic flow in Pb-Pb collisions at $\sqrt{s_{NN}} = 2.76$ TeV at the LHC”, *Eur. Phys. J. C* **77** (2017) 658, arXiv:1707.07304 [nucl-ex].
- [16] ALICE Collaboration, S. Acharya *et al.*, “Production of deuterons, tritons, ^3He nuclei, and their antinuclei in pp collisions at $\sqrt{s} = 0.9, 2.76,$ and 7 TeV”, *Phys. Rev. C* **97** (2018) 024615, arXiv:1709.08522 [nucl-ex].
- [17] ALICE Collaboration, S. Acharya *et al.*, “Production of ^4He and $^4\overline{\text{He}}$ in Pb-Pb collisions at $\sqrt{s_{NN}} = 2.76$ TeV at the LHC”, *Nucl. Phys. A* **971** (2018) 1–20, arXiv:1710.07531 [nucl-ex].
- [18] ALICE Collaboration, S. Acharya *et al.*, “Multiplicity dependence of light (anti-)nuclei production in p-Pb collisions at $\sqrt{s_{NN}} = 5.02$ TeV”, *Phys. Lett. B* **800** (2020) 135043, arXiv:1906.03136 [nucl-ex].
- [19] ALICE Collaboration, S. Acharya *et al.*, “Production of (anti-) ^3He and (anti-) ^3H in p-Pb collisions at $\sqrt{s_{NN}} = 5.02$ TeV”, *Phys. Rev. C* **101** (2020) 044906, arXiv:1910.14401 [nucl-ex].
- [20] ALICE Collaboration, S. Acharya *et al.*, “(Anti-)deuteron production in pp collisions at $\sqrt{s} = 13$ TeV”, *Eur. Phys. J. C* **80** (2020) 889, arXiv:2003.03184 [nucl-ex].
- [21] ALICE Collaboration, S. Acharya *et al.*, “Production of light (anti)nuclei in pp collisions at $\sqrt{s} = 13$ TeV”, *JHEP* **2022** (2022) 106, arXiv:2109.13026 [nucl-ex].
- [22] ALICE Collaboration, S. Acharya *et al.*, “Jet-associated deuteron production in pp collisions at $\sqrt{s} = 13$ TeV”, *Phys. Lett. B* **819** (2021) 136440, arXiv:2011.05898 [nucl-ex].
- [23] ALICE Collaboration, S. Acharya *et al.*, “Production of light (anti)nuclei in pp collisions at $\sqrt{s} = 5.02$ TeV”, *Eur. Phys. J. C* **82** (2022) 289, arXiv:2112.00610 [nucl-ex].
- [24] ALICE Collaboration, S. Acharya *et al.*, “Hypertriton Production in p-Pb collisions at $\sqrt{s_{NN}} = 5.02$ TeV”, *Phys. Rev. Lett.* **128** (2022) 252003, arXiv:2107.10627 [nucl-ex].
- [25] ALICE Collaboration, S. Acharya *et al.*, “Elliptic and triangular flow of (anti)deuterons in Pb-Pb collisions at $\sqrt{s_{NN}} = 5.02$ TeV”, *Phys. Rev. C* **102** (2020) 055203, arXiv:2005.14639 [nucl-ex].
- [26] ALICE Collaboration, S. Acharya *et al.*, “Measurement of the (anti-) ^3He elliptic flow in Pb-Pb collisions at $\sqrt{s_{NN}} = 5.02$ TeV”, *Phys. Lett. B* **805** (2020) 135414, arXiv:1910.09718 [nucl-ex].
- [27] ALICE Collaboration, S. Acharya *et al.*, “Enhanced Deuteron Coalescence Probability in Jets”, *Phys. Rev. Lett.* **131** (2023) 042301, arXiv:2211.15204 [nucl-ex]. Erratum: *Phys. Rev. Lett.* **132**, 109901 (2024).
- [28] ALICE Collaboration, S. Acharya *et al.*, “Measurement of the production of (anti)nuclei in p-Pb collisions at $\sqrt{s_{NN}} = 8.16$ TeV”, *Phys. Lett. B* **846** (2023) 137795, arXiv:2212.04777 [nucl-ex].

- [29] ALICE Collaboration, S. Acharya *et al.*, “First Measurement of Antideuteron Number Fluctuations at Energies Available at the Large Hadron Collider”, *Phys. Rev. Lett.* **131** (2023) 041901, arXiv:2204.10166 [nucl-ex].
- [30] ALICE Collaboration, S. Acharya *et al.*, “Light (anti)nuclei production in Pb-Pb collisions at $\sqrt{s_{NN}} = 5.02$ TeV”, *Phys. Rev. C* **107** (2023) 064904, arXiv:2211.14015 [nucl-ex].
- [31] J. Cleymans, S. Kabana, I. Kraus, H. Oeschler, K. Redlich, and N. Sharma, “Antimatter production in proton-proton and heavy-ion collisions at ultrarelativistic energies”, *Phys. Rev. C* **84** (2011) 054916, arXiv:1105.3719 [hep-ph].
- [32] A. Andronic, P. Braun-Munzinger, J. Stachel, and H. Stöcker, “Production of light nuclei, hypernuclei and their antiparticles in relativistic nuclear collisions”, *Phys. Lett. B* **697** (2011) 203–207, arXiv:1010.2995 [hep-ph].
- [33] F. Becattini, M. Bleicher, E. Grossi, J. Steinheimer, and R. Stock, “Centrality dependence of hadronization and chemical freeze-out conditions in heavy ion collisions at $\sqrt{s_{NN}} = 2.76$ TeV”, *Phys. Rev. C* **90** (2014) 054907, arXiv:1405.0710 [nucl-th].
- [34] V. Vovchenko and H. Stoecker, “Examination of the sensitivity of the thermal fits to heavy-ion hadron yield data to the modeling of the eigenvolume interactions”, *Phys. Rev. C* **95** (2017) 044904, arXiv:1606.06218 [hep-ph].
- [35] A. Andronic, P. Braun-Munzinger, K. Redlich, and J. Stachel, “Decoding the phase structure of QCD via particle production at high energy”, *Nature* **561** (2018) 321–330, arXiv:1710.09425 [nucl-th].
- [36] N. Sharma, J. Cleymans, B. Hippolyte, and M. Paradza, “A Comparison of pp, p–Pb, and Pb-Pb collisions in the thermal model: Multiplicity dependence of thermal parameters”, *Phys. Rev. C* **99** (2019) 044914, arXiv:1811.00399 [hep-ph].
- [37] V. Vovchenko, B. Dönigus, and H. Stoecker, “Canonical statistical model analysis of pp, p–Pb and Pb-Pb collisions at energies available at the CERN Large Hadron Collider”, *Phys. Rev. C* **100** (2019) 054906, arXiv:1906.03145 [hep-ph].
- [38] V. Vovchenko, B. Dönigus, and H. Stoecker, “Multiplicity dependence of light nuclei production at LHC energies in the canonical statistical model”, *Phys. Lett. B* **785** (2018) 171–174, arXiv:1808.05245 [hep-ph].
- [39] S. T. Butler and C. A. Pearson, “Deuterons from High-Energy Proton Bombardment of Matter”, *Phys. Rev.* **129** (1963) 836–842.
- [40] J. I. Kapusta, “Mechanisms for deuteron production in relativistic nuclear collisions”, *Phys. Rev. C* **21** (1980) 1301–1310.
- [41] R. Scheibl and U. Heinz, “Coalescence and flow in ultrarelativistic heavy ion collisions”, *Phys. Rev. C* **59** (1999) 1585–1602, arXiv:nucl-th/9809092 [nucl-th].
- [42] W. Zhao, L. Zhu, H. Zheng, C. M. Ko, and H. Song, “Spectra and flow of light nuclei in relativistic heavy ion collisions at energies available at the BNL Relativistic Heavy Ion Collider and at the CERN Large Hadron Collider”, *Phys. Rev. C* **98** (2018) 054905, arXiv:1807.02813 [nucl-th].
- [43] K. Blum and M. Takimoto, “Nuclear coalescence from correlation functions”, *Phys. Rev. C* **99** (2019) 044913, arXiv:1901.07088 [nucl-th].

- [44] K.-J. Sun, C. M. Ko, and B. Dönigus, “Suppression of light nuclei production in collisions of small systems at the Large Hadron Collider”, *Phys. Lett. B* **792** (2019) 132–137, arXiv:1812.05175 [nucl-th].
- [45] M. Kachelrieß, S. Ostapchenko, and J. Tjemsland, “Alternative coalescence model for deuteron, tritium, helium-3 and their antinuclei”, *The European Physical Journal A* **56** (2020) 4, arXiv:1905.01192 [hep-ph].
- [46] M. Mahlein, L. Barioglio, F. Bellini, L. Fabbietti, C. Pinto, B. Singh, and S. Tripathy, “A realistic coalescence model for deuteron production”, *Eur. Phys. J. C* **83** (2023) 804, arXiv:2302.12696 [hep-ex].
- [47] A. Kounine, “The Alpha Magnetic Spectrometer on the International Space Station”, *Int. J. of Mod. Phys. E* **21** (2012) 1230005.
- [48] C. J. Hailey, “An indirect search for dark matter using antideuterons: the GAPS experiment”, *New J. Phys.* **11** (2009) 105022.
- [49] F. Donato, N. Fornengo, and D. Maurin, “Antideuteron fluxes from dark matter annihilation in diffusion models”, *Phys. Rev. D* **78** (2008) 043506, arXiv:0803.2640 [hep-ex].
- [50] M. Korsmeier, F. Donato, and N. Fornengo, “Prospects to verify a possible dark matter hint in cosmic antiprotons with antideuterons and antihelium”, *Phys. Rev. D* **97** (2018) 103011, arXiv:1711.08465 [astro-ph.HE].
- [51] AMS Collaboration, M. Aguilar *et al.*, “Antiproton Flux, Antiproton-to-Proton Flux Ratio, and Properties of Elementary Particle Fluxes in Primary Cosmic Rays Measured with the Alpha Magnetic Spectrometer on the International Space Station”, *Phys. Rev. Lett.* **117** (2016) 091103.
- [52] ALICE Collaboration, S. Acharya *et al.*, “Measurement of the Low-Energy Antideuteron Inelastic Cross Section”, *Phys. Rev. Lett.* **125** (2020) 162001, arXiv:2005.11122 [nucl-ex].
- [53] ALICE Collaboration, S. Acharya *et al.*, “Measurement of the low-energy antitriton inelastic cross section”, *Physics Letters B* **848** (2024) 138337, arXiv:2307.03603 [nucl-ex]. <https://www.sciencedirect.com/science/article/pii/S0370269323006718>.
- [54] ALICE Collaboration, S. Acharya *et al.*, “Measurement of anti- ^3He nuclei absorption in matter and impact on their propagation in the Galaxy”, *Nature Physics* **19** (2022) 61–71, arXiv:2202.01549 [nucl-ex].
- [55] N. Sharma, T. Perez, A. Castro, L. Kumar, and C. Nattrass, “Methods for separation of deuterons produced in the medium and in jets in high energy collisions”, *Phys. Rev. C* **98** (2018) 014914, arXiv:1803.02313 [hep-ph].
- [56] ALICE Collaboration, S. Acharya *et al.*, “Measurement of jet radial profiles in Pb–Pb collisions at $\sqrt{s_{\text{NN}}} = 2.76$ TeV”, *Phys. Lett. B* **796** (2019) 204–219, arXiv:1904.13118 [nucl-ex].
- [57] F. Bellini, K. Blum, A. P. Kalweit, and M. Puccio, “Examination of coalescence as the origin of nuclei in hadronic collisions”, *Phys. Rev. C* **103** (2021) 014907, arXiv:2007.01750 [nucl-th].
- [58] S. Sapeta, “QCD and Jets at Hadron Colliders”, *Prog. Part. Nucl. Phys.* **89** (2016) 1–55, arXiv:1511.09336 [hep-ph].
- [59] ALICE Collaboration, S. Acharya *et al.*, “Production of K_S^0 , Λ ($\bar{\Lambda}$), Ξ^\pm and Ω^\pm in jets and in the underlying event in pp and p–Pb collisions”, *JHEP* **07** (2023) 136, arXiv:2211.08936 [nucl-ex].

- [60] **ALICE** Collaboration, S. Acharya *et al.*, “Production of Λ and K_s^0 in jets in p–Pb collisions at $\sqrt{s_{NN}}=5.02$ TeV and pp collisions at $\sqrt{s}=7$ TeV”, *Phys. Lett. B* **827** (2022) 136984, arXiv:2105.04890 [nucl-ex].
- [61] **ALICE** Collaboration, S. Acharya *et al.*, “Underlying-event properties in pp and p–Pb collisions at $\sqrt{s_{NN}} = 5.02$ TeV”, *JHEP* **06** (2023) 023, arXiv:2204.10389 [nucl-ex].
- [62] **ALICE** Collaboration, S. Acharya *et al.*, “Underlying event properties in pp collisions at $\sqrt{s} = 13$ TeV”, *JHEP* **4** (2020) 192, arXiv:1910.14400 [nucl-ex].
- [63] **ALICE** Collaboration, K. Aamodt *et al.*, “The ALICE experiment at the CERN LHC”, *JINST* **3** (2008) S08002.
- [64] **ALICE** Collaboration, B. Abelev *et al.*, “Performance of the ALICE experiment at the CERN LHC”, *Int. J. Mod. Phys. A* **29** (2014) 1430044, arXiv:1402.4476 [nucl-ex].
- [65] J. Alme *et al.*, “The ALICE TPC, a large 3-dimensional tracking device with fast readout for ultra-high multiplicity events”, *Nucl. Instrum. Meth. A* **622** (2010) 316–367, arXiv:1001.1950 [physics.ins-det].
- [66] A. Akindinov *et al.*, “Performance of the ALICE Time-Of-Flight detector at the LHC”, *Eur. Phys. J. Plus* **128** (2013) 44.
- [67] **ALICE** Collaboration, J. Adam *et al.*, “Determination of the event collision time with the ALICE detector at the LHC”, *Eur. Phys. J. Plus* **132** (2017) 99, arXiv:1610.03055 [physics.ins-det].
- [68] **ALICE** Collaboration, P. Cortese *et al.*, “ALICE technical design report on forward detectors: FMD, T0 and V0”, (2004) CERN–LHCC–2004–025.
- [69] X.-N. Wang and M. Gyulassy, “HIJING: A Monte Carlo model for multiple jet production in pp, pA and AA collisions”, *Phys. Rev. D* **44** (1991) 3501–3516.
- [70] **GEANT4** Collaboration, S. Agostinelli *et al.*, “GEANT4 - A Simulation Toolkit”, *Nucl. Instrum. Meth. A* **506** (2003) 250–303.
- [71] S. Roesler, R. Engel, and J. Ranft, “The Monte Carlo event generator DPMJET-III”, in *International Conference on Advanced Monte Carlo for Radiation Physics, Particle Transport Simulation and Applications*, pp. 1033–1038. 12, 2000. arXiv:hep-ph/0012252.
- [72] P. Schwaller, M. Pepin, B. Favier, C. Richard-Serre, D. F. Measday, and P. U. Renberg, “Proton total cross-sections on ^1H , ^2H , ^4He , ^9Be , C and O in the energy range 180 MeV to 560 MeV”, *Nucl. Phys. A* **316** (1979) 317–344.
- [73] W. Bauhoff, “Tables of reaction and total cross sections for proton-nucleus scattering below 1 GeV”, *Atomic Data and Nuclear Data Tables* **35** (1986) 429–447.
- [74] B. M. Bobchenko *et al.*, “Measurement of total inelastic cross-sections from proton interactions with nuclei in the momentum range from 5 GeV/c to 9 GeV/c and pi-mesons with nuclei in the momentum range from 1.75 GeV/c to 6.5 GeV/c”, *Sov. J. Nucl. Phys.* **30** (1979) 805.
- [75] J. Jaros, A. Wagner, *et al.*, “Nucleus-nucleus total cross sections for light nuclei at 1.55 and 2.89 GeV/c per nucleon”, *Phys. Rev. C* **18** (1978) 2273–2292.
- [76] A. Bianconi, M. Corradini, *et al.*, “Measurement of the antiproton–nucleus annihilation cross section at 5.3 MeV”, *Phys. Lett. B* **704** (2011) 461–466.

- [77] V. Kuzichev, Y. Lepikhin, and V. Smirnitsky, “The antiproton-nuclei annihilation cross-section at the momentum range from 0.70 to 2.50 GeV/c”, Nuc. Phys. A **576** (1994) 581–602.
- [78] K. Nakamura, J. Chiba, T. Fujii, H. Iwasaki, T. Kageyama, S. Kuribayashi, T. Sumiyoshi, T. Takeda, H. Ikeda, and Y. Takada, “Absorption and Forward Scattering of Antiprotons by C, Al, and Cu Nuclei in the Region 470-880 MeV/c”, Phys. Rev. Lett. **52** (1984) 731–734.
- [79] V. Ashford, M. E. Sainio, M. Sakitt, J. Skelly, R. Debbe, W. Fickinger, R. Marino, and D. K. Robinson, “Low energy antiproton nuclear absorption cross sections”, Phys. Rev. C **31** (1985) 663–665.
- [80] A. Auce, R. F. Carlson, A. J. Cox, A. Ingemarsson, R. Johansson, P. U. Renberg, O. Sundberg, and G. Tibell, “Reaction cross sections for 38, 65, and 97 MeV deuterons on targets from ^9Be to ^{208}Pb ”, Phys. Rev. C **53** (1996) 2919–2925.
- [81] C. Tsallis, “Possible Generalization of Boltzmann-Gibbs Statistics”, J. Statist. Phys. **52** (1988) 479–487.
- [82] ALICE Collaboration, S. Acharya et al., “Multiplicity dependence of charged-particle jet production in pp collisions at $\sqrt{s} = 13 \text{ TeV}$ ”, Eur. Phys. J. C **82** (2022) 514, arXiv:2202.01548 [nucl-ex].
- [83] ALICE Collaboration, S. A. et al, “Unveiling the strong interaction among hadrons at the LHC”, Nature **588** (2020) 232–238, arXiv:2005.11495 [nucl-ex]. [Erratum: Nature 590, E13 (2021)].
- [84] ALICE Collaboration, S. Acharya et al., “ $p - p$, $p - \Lambda$, and $\Lambda - \Lambda$ correlations studied via femtoscopy in pp reactions at $\sqrt{s} = 7 \text{ TeV}$ ”, Phys. Rev. C **99** (2019) 024001, arXiv:1805.12455 [nucl-ex].
- [85] ALICE Collaboration, S. Acharya et al., “First Observation of an Attractive Interaction between a Proton and a Cascade Baryon”, Phys. Rev. Lett. **123** (2019) 112002, arXiv:1904.12198 [nucl-ex].
- [86] C. Bierlich et al., “A comprehensive guide to the physics and usage of PYTHIA 8.3”, SciPost Phys. Codeb. **2022** (2022) 8, arXiv:2203.11601 [hep-ph].
- [87] C. Bierlich, G. Gustafson, L. Lönnblad, and H. Shah, “The Angantyr model for Heavy-Ion Collisions in PYTHIA8”, JHEP **10** (2018) 134, arXiv:1806.10820 [hep-ph].
- [88] B. Andersson, G. Gustafson, and B. Nilsson-Almqvist, “A Model for Low p(t) Hadronic Reactions, with Generalizations to Hadron - Nucleus and Nucleus-Nucleus Collisions”, Nucl. Phys. B **281** (1987) 289–309.
- [89] H. Pi, “An Event generator for interactions between hadrons and nuclei: FRITIOF version 7.0”, Comput. Phys. Commun. **71** (1992) 173–192.
- [90] ALICE Collaboration, S. Acharya et al., “Observation of deuteron and antideuteron formation from resonance-decay nucleons”, Nature **648** (2025) 306–311.
- [91] ALICE Collaboration, S. Acharya et al., “Production of pions, kaons, and protons as a function of the relative transverse activity classifier in pp collisions at $\sqrt{s} = 13 \text{ TeV}$ ”, JHEP **06** (2023) 027, arXiv:2301.10120 [nucl-ex].

A The ALICE Collaboration

D.A.H. Abdallah¹³⁴, I.J. Abualrob¹¹², S. Acharya⁴⁹, G. Aglieri Rinella³², L. Aglietta²⁴, N. Agrawal²⁵, Z. Ahammed¹³², S. Ahmad¹⁵, I. Ahuja³⁶, Z. Akbar⁷⁹, V. Akishina³⁸, M. Al-Turany⁹⁴, B. Alessandro⁵⁵, R. Alfaro Molina⁶⁶, B. Ali¹⁵, A. Alici^{1,25}, J. Alme²⁰, G. Alocco²⁴, T. Alt⁶³, I. Altsybeev⁹², C. Andrei⁴⁴, N. Andreou¹¹¹, A. Andronic¹²³, M. Angeletti³², V. Angelov⁹¹, F. Antinori⁵³, P. Antonioli⁵⁰, N. Apadula⁷¹, H. Appelshäuser⁶³, S. Arcelli^{1,25}, R. Arnaldi⁵⁵, I.C. Arsene¹⁹, M. Arslandok¹³⁵, A. Augustinus³², R. Averbeck⁹⁴, M.D. Azmi¹⁵, H. Baba¹²¹, A.R.J. Babu¹³⁴, A. Badalà⁵², J. Bae¹⁰⁰, Y. Bae¹⁰⁰, Y.W. Baek¹⁰⁰, X. Bai¹¹⁶, R. Bailhache⁶³, Y. Bailung¹²⁵, R. Bala⁸⁸, A. Baldisseri¹²⁷, B. Balis², S. Bangalia¹¹⁴, Z. Banoo⁸⁸, V. Barbasova³⁶, F. Barile³¹, L. Barioglio⁵⁵, M. Barlou²⁴, B. Barman⁴⁰, G.G. Barnaföldi⁴⁵, L.S. Barnby¹¹¹, E. Barreau⁹⁹, V. Barret¹²⁴, L. Barreto¹⁰⁶, K. Barth³², E. Bartsch⁶³, N. Bastid¹²⁴, G. Batigne⁹⁹, D. Battistini^{34,92}, B. Batyunya¹³⁹, L. Baudino²⁴, D. Bauri⁴⁶, J.L. Bazo Alba⁹⁸, I.G. Bearden⁸⁰, P. Becht⁹⁴, D. Behera^{77,47}, S. Behera⁴⁶, I. Belikov¹²⁶, V.D. Bella¹²⁶, F. Bellini²⁵, R. Bellwied¹¹², L.G.E. Beltran¹⁰⁵, Y.A.V. Beltran⁴³, G. Bencedi⁴⁵, O. Benchikhi⁷³, A. Bensaoula¹¹², S. Beole²⁴, A. Berdnikova⁹¹, L. Bergmann⁷¹, L. Bernardinis²³, L. Betev³², P.P. Bhaduri¹³², T. Bhalla⁸⁷, A. Bhasin⁸⁸, B. Bhattacharjee⁴⁰, L. Bianchi²⁴, J. Bielčik³⁴, J. Bielčíková⁸³, A. Bilandzic⁹², A. Binoy¹¹⁴, G. Biro⁴⁵, S. Biswas⁴, M.B. Blidaru⁹⁴, N. Bluhme³⁸, C. Blume⁶³, F. Bock⁸⁴, T. Bodova²⁰, L. Boldizsár⁴⁵, M. Bombara³⁶, P.M. Bond³², G. Bonomi^{131,54}, H. Borel¹²⁷, A. Borissov¹³⁹, A.G. Borquez Carcamo⁹¹, E. Botta²⁴, N. Bouchhar¹⁷, Y.E.M. Bouziani⁶³, D.C. Brandibur⁶², L. Bratrud⁶³, P. Braun-Munzinger⁹⁴, M. Bregant¹⁰⁶, M. Broz³⁴, G.E. Bruno^{93,31}, V.D. Buchakchiev³⁵, M.D. Buckland⁸², H. Buesching⁶³, S. Bufalino²⁹, P. Buhler⁷³, N. Burmasov¹³⁹, Z. Buthelezi^{67,120}, A. Bylinkin²⁰, C. Carr⁹⁷, J.C. Cabanillas Noris¹⁰⁵, M.F.T. Cabrera¹¹², H. Caines¹³⁵, A. Caliva²⁸, E. Calvo Villar⁹⁸, J.M.M. Camacho¹⁰⁵, P. Camerini²³, M.T. Camerlingo⁴⁹, F.D.M. Canedo¹⁰⁶, S. Cannito²³, S.L. Cantway¹³⁵, M. Carabas¹⁰⁹, F. Carnesecchi³², L.A.D. Carvalho¹⁰⁶, J. Castillo Castellanos¹²⁷, M. Castoldi³², F. Catalano³², S. Cattaruzzi²³, R. Cerri²⁴, I. Chakaberia⁷¹, P. Chakraborty¹³³, J.W.O. Chan¹¹², S. Chandra¹³², S. Chapeland³², M. Chartier¹¹⁵, S. Chattopadhyay¹³², M. Chen³⁹, T. Cheng⁶, M.I. Cherciu⁶², C. Cheshkov¹²⁵, D. Chiappara²⁷, V. Chibante Barroso³², D.D. Chinellato⁷³, F. Chinu²⁴, E.S. Chizzali^{11,92}, J. Cho⁵⁷, S. Cho⁵⁷, P. Chochula³², Z.A. Chochulska^{113,133}, P. Christakoglou⁸¹, C.H. Christensen⁸⁰, P. Christiansen⁷², T. Chujo¹²², B. Chytla¹³³, M. Ciaccio²⁴, C. Cicalo⁵¹, G. Cimaror^{32,24}, F. Cindolo⁵⁰, F. Colamaria⁴⁹, D. Colella³¹, A. Colelli³¹, M. Colocci²⁵, M. Concas³², G. Conesa Balbastre⁷⁰, Z. Conesa del Valle¹²⁸, G. Contin²³, J.G. Contreras³⁴, M.L. Coquet⁹⁹, P. Cortese^{130,55}, M.R. Cosentino¹⁰⁸, F. Costa³², S. Costanza²¹, P. Crochet¹²⁴, M.M. Czarnynoga¹³³, A. Dainese⁵³, E. Dall'occo³², G. Dange³⁸, M.C. Danisch¹⁶, A. Danu⁶², A. Daribayeva³⁸, P. Das³², S. Das⁴, A.R. Dash¹²³, S. Dash⁴⁶, A. De Caro²⁸, G. de Cataldo⁴⁹, J. de Cuveland³⁸, A. De Falco²², D. De Gruttola²⁸, N. De Marco⁵⁵, C. De Martin²³, S. De Pasquale²⁸, R. Deb¹³¹, R. Del Grande³⁴, L. Dello Stritto³², G.G.A. de Souza^{IV,106}, P. Dhankher¹⁸, D. Di Bari³¹, M. Di Costanzo²⁹, A. Di Mauro³², B. Di Ruzza^{I,129,49}, B. Diab³², Y. Ding⁶, J. Ditzel⁶³, R. Divià³², U. Dmitrieva⁵⁵, A. Dobrin⁶², B. Dönigus⁶³, L. Döpper⁴¹, L. Drzensla², J.M. Dubinski¹³³, A. Dubla⁹⁴, P. Dupieux¹²⁴, N. Dzalaiova¹³, T.M. Eder¹²³, R.J. Ehlers⁷¹, F. Eisenhut⁶³, R. Ejima⁸⁹, D. Elia⁴⁹, B. Erazmus⁹⁹, F. Ercolessi²⁵, B. Espagnon¹²⁸, G. Eulisse³², D. Evans⁹⁷, L. Fabbietti⁹², G. Fabbri⁵⁰, M. Faggin³², J. Faivre⁷⁰, W. Fan¹¹², T. Fang⁶, A. Fantoni⁴⁸, A. Feliciello⁵⁵, W. Feng⁶, A. Fernández Téllez⁴³, B. Fernando¹³⁴, L. Ferrandi¹⁰⁶, A. Ferrero¹²⁷, C. Ferrero^{V,55}, A. Ferretti²⁴, D. Finogeev¹³⁹, F.M. Fionda⁵¹, A.N. Flores¹⁰⁴, S. Foertsch⁶⁷, I. Fokin⁹¹, U. Follo^{V,55}, R. Forynski¹¹¹, E. Fragiaco⁵⁶, H. Friberg⁹², U. Fuchs³², D. Fuligno²³, N. Funicello²⁸, C. Furget⁷⁰, A. Furs¹³⁹, T. Fusayasu⁹⁵, J.J. Gaardhøje⁸⁰, M. Gagliardi²⁴, A.M. Gago⁹⁸, T. Gahlaut⁴⁶, C.D. Galvan¹⁰⁵, S. Gami⁷⁷, C. Garabatos⁹⁴, J.M. Garcia⁴³, E. Garcia-Solis⁹, S. Garetti¹²⁸, C. Gargiulo³², P. Gasik⁹⁴, A. Gautam¹¹⁴, M.B. Gay Ducati⁶⁵, M. Germain⁹⁹, R.A. Gernhaeuser⁹², M. Giacalone³², G. Gioachin²⁹, S.K. Giri¹³², P. Giubellino⁵⁵, P. Giubilato²⁷, P. Glässel⁹¹, E. Glimos¹¹⁹, L. Gonella²³, V. Gonzalez¹³⁴, M. Gorgon², K. Goswami⁴⁷, S. Gotovac³³, V. Grabski⁶⁶, L.K. Graczykowski¹³³, E. Grecka⁸³, A. Grelli⁵⁸, C. Grigoras³², S. Grigoryan^{139,1}, O.S. Groettvik³², F. Grosa³², S. Gross-Börling⁹⁴, J.F. Grosse-Oetringhaus³², R. Grosso⁹⁴, D. Grund³⁴, N.A. Grunwald⁹¹, R. Guernane⁷⁰, M. Guilbaud⁹⁹, K. Gulbrandsen⁸⁰, J.K. Gumprecht⁷³, T. Gündem⁶³, T. Gunji¹²¹, J. Guo¹⁰, W. Guo⁶, A. Gupta⁸⁸, R. Gupta⁸⁸, R. Gupta⁴⁷, K. Gwizdziel¹³³, L. Gyulai⁴⁵, T. Hachiya⁷⁵, C. Hadjidakis¹²⁸, F.U. Haider⁸⁸,

S. Haidlova³⁴, M. Haldar⁴, W. Ham¹⁰⁰, H. Hamagaki⁷⁴, Y. Han¹³⁷, R. Hannigan¹⁰⁴, J. Hansen⁷², J.W. Harris¹³⁵, A. Harton⁹, M.V. Hartung⁶³, A. Hasan¹¹⁸, H. Hassan¹¹³, D. Hatzifotiadiou⁵⁰, P. Hauer⁴¹, L.B. Havener¹³⁵, E. Hellbär³², H. Helstrup³⁷, M. Hemmer⁶³, S.G. Hernandez¹¹², G. Herrera Corral⁸, K.F. Hetland³⁷, B. Heybeck⁶³, H. Hillemanns³², B. Hippolyte¹²⁶, I.P.M. Hobus⁸¹, F.W. Hoffmann³⁸, B. Hofman⁵⁸, Y. Hong⁵⁷, A. Horzyk², Y. Hou^{94,11}, P. Hristov³², L.M. Huhta¹¹³, T.J. Humanic⁸⁵, V. Humlova³⁴, M. Husar⁸⁶, A. Hutson¹¹², D. Hutter³⁸, M.C. Hwang¹⁸, M. Inaba¹²², A. Isakov⁸¹, T. Isidori¹¹⁴, M.S. Islam⁴⁶, M. Ivanov⁹⁴, M. Ivanov¹³, K.E. Iversen⁷², J.G. Kim¹³⁷, M. Jablonski², B. Jacak^{18,71}, N. Jacazio²⁵, P.M. Jacobs⁷¹, A. Jadlovská¹⁰², S. Jadlovská¹⁰², S. Jaelani⁷⁹, C. Jahnke¹⁰⁷, M.J. Jakubowska¹³³, E.P. Jamro², D.M. Janik³⁴, M.A. Janik¹³³, S. Ji¹⁶, Y. Ji⁹⁴, S. Jia⁸⁰, T. Jiang¹⁰, A.A.P. Jimenez⁶⁴, S. Jin¹⁰, F. Jonas⁷¹, D.M. Jones¹¹⁵, J.M. Jowett^{32,94}, J. Jung⁶³, M. Jung⁶³, A. Junique³², J. Juracka³⁴, J. Kaewjai^{115,101}, P. Kalinak⁵⁹, A. Kalweit³², A. Karasu Uysal¹³⁶, N. Karatzenis⁹⁷, T. Karavicheva¹³⁹, M.J. Karwowska¹³³, V. Kashyap⁷⁷, M. Keil³², B. Ketzer⁴¹, J. Keul⁶³, S.S. Khade⁴⁷, A.M. Khan¹¹⁶, A. Khuntia⁵⁰, Z. Khuranova⁶³, B. Kileng³⁷, B. Kim¹⁰⁰, D.J. Kim¹¹³, D. Kim¹⁰⁰, E.J. Kim⁶⁸, G. Kim⁵⁷, H. Kim⁵⁷, J. Kim¹³⁷, J. Kim⁵⁷, J. Kim³², M. Kim¹⁸, S. Kim¹⁷, T. Kim¹³⁷, J.T. Kinner¹²³, I. Kisel³⁸, A. Kisiel¹³³, J.L. Klay⁵, J. Klein³², S. Klein⁷¹, C. Klein-Bösing¹²³, M. Kleiner⁶³, A. Kluge³², M.B. Knuesel¹³⁵, C. Kobdaj¹⁰¹, R. Kohara¹²¹, A. Kondratyev¹³⁹, J. König⁶³, P.J. Konopka³², G. Kornakov¹³³, M. Korwieser⁹², C. Koster⁸¹, A. Kotliarov⁸³, N. Kovacic⁸⁶, M. Kowalski¹⁰³, V. Kozhuharov³⁵, G. Kozlov³⁸, I. Králik⁵⁹, A. Kravčáková³⁶, M.A. Krawczyk³², L. Krcal³², F. Krizek⁸³, K. Krizkova Gajdosova³⁴, C. Krug⁶⁵, M. Krüger⁶³, E. Kryshen¹³⁹, V. Kučera⁵⁷, C. Kuhn¹²⁶, D. Kumar¹³², L. Kumar⁸⁷, N. Kumar⁸⁷, S. Kumar⁴⁹, S. Kundu³², M. Kuo¹²², P. Kurashvili⁷⁶, S. Kurita⁸⁹, S. Kushpil⁸³, A. Kuznetsov¹³⁹, M.J. Kweon⁵⁷, Y. Kwon¹³⁷, S.L. La Pointe³⁸, P. La Rocca²⁶, A. Lakrathok¹⁰¹, S. Lambert⁹⁹, A.R. Landou⁷⁰, R. Langoy¹¹⁸, P. Larionov³², E. Laudi³², L. Lautner⁹², R.A.N. Laveaga¹⁰⁵, R. Lavicka⁷³, R. Lea^{131,54}, J.B. Lebert³⁸, H. Lee¹⁰⁰, S. Lee⁵⁷, I. Legrand⁴⁴, G. Legras¹²³, A.M. Lejeune³⁴, T.M. Lelek², I. León Monzón¹⁰⁵, M.M. Lesch⁹², P. Lévai⁴⁵, M. Li⁶, P. Li¹⁰, X. Li¹⁰, B.E. Liang-Gilman¹⁸, J. Lien¹¹⁸, R. Lietava⁹⁷, I. Likmeta¹¹², B. Lim⁵⁵, H. Lim¹⁶, S.H. Lim¹⁶, Y.N. Lima¹⁰⁶, S. Lin¹⁰, V. Lindenstruth³⁸, C. Lippmann⁹⁴, D. Liskova¹⁰², D.H. Liu⁶, J. Liu¹¹⁵, Y. Liu⁶, G.S.S. Liveraro¹⁰⁷, I.M. Lofnes²⁰, C. Loizides²⁰, S. Lokos¹⁰³, J. Lömker⁵⁸, X. Lopez¹²⁴, E. López Torres⁷, C. Lotteau¹²⁵, P. Lu¹¹⁶, W. Lu⁶, Z. Lu¹⁰, O. Lubyets⁹⁴, G.A. Lucia²⁹, F.V. Lugo⁶⁶, J. Luo³⁹, G. Luparello⁵⁶, J. M. Friedrich⁹², Y.G. Ma³⁹, V. Machacek⁸⁰, M. Mager³², M. Mahlein⁹², A. Maire¹²⁶, E. Majerz², M.V. Makariev³⁵, G. Malfattore⁵⁰, N.M. Malik⁸⁸, N. Malik¹⁵, D. Mallick¹²⁸, N. Mallick¹¹³, G. Mandaglio^{30,52}, S. Mandal⁷⁷, S.K. Mandal⁷⁶, A. Manea⁶², R. Manhart⁹², A.K. Manna⁴⁷, F. Manso¹²⁴, G. Mantzaridis⁹², V. Manzari⁴⁹, Y. Mao⁶, R.W. Marcjan², G.V. Margagliotti²³, A. Margotti⁵⁰, A. Marín⁹⁴, C. Markert¹⁰⁴, P. Martinengo³², M.I. Martínez⁴³, M.P.P. Martins^{32,106}, S. Masciocchi⁹⁴, M. Masera²⁴, A. Masoni⁵¹, L. Massacrier¹²⁸, O. Massen⁵⁸, A. Mastroserio^{129,49}, L. Mattei^{24,124}, S. Mattiazzo²⁷, A. Matyja¹⁰³, J.L. Mayo¹⁰⁴, F. Mazzaschi³², M. Mazzilli³¹, Y. Melikyan⁴², M. Melo¹⁰⁶, A. Menchaca-Rocha⁶⁶, J.E.M. Mendez⁶⁴, E. Meninno⁷³, M.W. Menzel^{32,91}, M. Meres¹³, L. Micheletti⁵⁵, D. Mihai¹⁰⁹, D.L. Mihaylov⁹², A.U. Mikalsen²⁰, K. Mikhaylov¹³⁹, L. Millot⁷⁰, N. Minafra¹¹⁴, D. Miśkowiec⁹⁴, A. Modak⁵⁶, B. Mohanty⁷⁷, M. Mohisin Khan^{VI,15}, M.A. Molander⁴², M.M. Mondal⁷⁷, S. Monira¹³³, D.A. Moreira De Godoy¹²³, A. Morsch³², C. Moscatelli²³, T. Mrnjavac³², S. Mrozinski⁶³, V. Muccifora⁴⁸, S. Muhuri¹³², A. Mulliri²², M.G. Munhoz¹⁰⁶, R.H. Munzer⁶³, L. Musa³², J. Musinsky⁵⁹, J.W. Myrcha¹³³, B. Naik¹²⁰, A.I. Nambrath¹⁸, B.K. Nandi⁴⁶, R. Nania⁵⁰, E. Nappi⁴⁹, A.F. Nassirpour¹⁷, V. Nastase¹⁰⁹, A. Nath⁹¹, N.F. Nathanson⁸⁰, A. Neagu¹⁹, L. Nellen⁶⁴, R. Nepeivoda⁷², S. Nese¹⁹, N. Nicassio³¹, B.S. Nielsen⁸⁰, E.G. Nielsen⁸⁰, F. Noferini⁵⁰, S. Noh¹², P. Nomokonov¹³⁹, J. Norman¹¹⁵, N. Novitzky⁸⁴, J. Nystrand²⁰, M.R. Ockleton¹¹⁵, M. Ogino⁷⁴, J. Oh¹⁶, S. Oh¹⁷, A. Ohlson⁷², M. Oida⁸⁹, L.A.D. Oliveira^{I,107}, C. Oppedisano⁵⁵, A. Ortiz Velasquez⁶⁴, H. Osanai⁷⁴, J. Otwinowski¹⁰³, M. Oya⁸⁹, K. Oyama⁷⁴, S. Padhan^{131,46}, D. Pagano^{131,54}, V. Pagliarino⁵⁵, G. Paić⁶⁴, A. Palasciano^{93,49}, I. Panasenکو⁷², P. Panigrahi⁴⁶, C. Pantouvakis²⁷, H. Park¹²², J. Park¹²², S. Park¹⁰⁰, T.Y. Park¹³⁷, J.E. Parkkila¹³³, P.B. Pati⁸⁰, Y. Patley⁴⁶, R.N. Patra⁴⁹, B. Paul¹³², F. Pazdic⁹⁷, H. Pei⁶, T. Peitzmann⁵⁸, X. Peng^{53,11}, S. Perciballi²⁴, G.M. Perez⁷, M. Petrovici⁴⁴, S. Piano⁵⁶, M. Pikna¹³, P. Pillot⁹⁹, O. Pinazza^{50,32}, C. Pinto³², S. Pisano⁴⁸, M. Płoskoń⁷¹, A. Plachta¹³³, M. Planinic⁸⁶, D.K. Plociennik², S. Politano³², N. Poljak⁸⁶, A. Pop⁴⁴, S. Porteboeuf-Houssais¹²⁴, J.S. Potgieter¹¹⁰, I.Y. Pozos⁴³, K.K. Pradhan⁴⁷, S.K. Prasad⁴, S. Prasad⁴⁷, R. Preghenella⁵⁰,

F. Prino ⁵⁵, C.A. Pruneau ¹³⁴, M. Puccio ³², S. Pucillo ²⁸, S. Pulawski ¹¹⁷, L. Quaglia ²⁴, A.M.K. Radhakrishnan ⁴⁷, S. Ragoni ¹⁴, A. Rai ¹³⁵, A. Rakotozafindrabe ¹²⁷, N. Ramasubramanian ¹²⁵, L. Ramello ^{130,55}, C.O. Ramírez-Álvarez ⁴³, M. Rasa ²⁶, S.S. Räsänen ⁴², R. Rath ⁹⁴, M.P. Rauch ²⁰, I. Ravasenga ³², M. Razza ²⁵, K.F. Read ^{84,119}, C. Reckziegel ¹⁰⁸, A.R. Redelbach ³⁸, K. Redlich ^{7,76}, C.A. Reetz ⁹⁴, H.D. Regules-Medel ⁴³, A. Rehman ²⁰, F. Reidt ³², H.A. Reme-Ness ³⁷, K. Reygers ⁹¹, M. Richter ²⁰, A.A. Riedel ⁹², W. Riegler ³², A.G. Riffero ²⁴, M. Rignanese ²⁷, C. Ripoli ²⁸, C. Ristea ⁶², M.V. Rodríguez ³², M. Rodríguez Cahuantzi ⁴³, K. Røed ¹⁹, E. Rogochaya ¹³⁹, D. Rohr ³², D. Röhrich ²⁰, S. Rojas Torres ³⁴, P.S. Rokita ¹³³, G. Romanenko ²⁵, F. Ronchetti ³², D. Rosales Herrera ⁴³, E.D. Rosas ⁶⁴, K. Roslon ¹³³, A. Rossi ⁵³, A. Roy ⁴⁷, A. Roy ¹¹⁸, S. Roy ⁴⁶, N. Rubini ⁵⁰, O. Rubza ^{1,15}, J.A. Rudolph ⁸¹, D. Ruggiano ¹³³, R. Rui ²³, P.G. Russek ², A. Rustamov ⁷⁸, A. Rybicki ¹⁰³, L.C.V. Ryder ¹¹⁴, G. Ryu ⁶⁹, J. Ryu ¹⁶, W. Rzesza ⁹², B. Sabiu ⁵⁰, R. Sadek ⁷¹, S. Sadhu ⁴¹, A. Saha ³¹, S. Saha ⁷⁷, B. Sahoo ⁴⁷, R. Sahoo ⁴⁷, D. Sahu ⁶⁴, P.K. Sahu ⁶⁰, J. Saini ¹³², S. Sakai ¹²², S. Sambyal ⁸⁸, D. Samitz ⁷³, I. Sanna ³², D. Sarkar ⁸⁰, V. Sarritzu ²², V.M. Sarti ⁹², M.H.P. Sas ⁸¹, U. Savino ²⁴, S. Sawan ⁷⁷, E. Scapparone ⁵⁰, J. Schambach ⁸⁴, H.S. Scheid ³², C. Schiaua ⁴⁴, R. Schicker ⁹¹, F. Schlepfer ^{32,91}, A. Schmah ⁹⁴, C. Schmidt ⁹⁴, M. Schmidt ⁹⁰, J. Schoengarth ⁶³, R. Schotter ⁷³, A. Schröter ³⁸, J. Schukraft ³², K. Schweda ⁹⁴, G. Scioli ²⁵, E. Scomparin ⁵⁵, J.E. Seger ¹⁴, D. Sekihata ¹²¹, M. Selina ⁸¹, I. Selyuzhenkov ⁹⁴, S. Senyukov ¹²⁶, J.J. Seo ⁹¹, L. Serkin ^{8,64}, L. Šeršňytė ³², A. Sevcenco ⁶², T.J. Shaba ⁶⁷, A. Shabetai ⁹⁹, R. Shahoyan ³², B. Sharma ⁸⁸, D. Sharma ⁴⁶, H. Sharma ⁵³, M. Sharma ⁸⁸, S. Sharma ⁸⁸, T. Sharma ⁴⁰, U. Sharma ⁸⁸, O. Sheibani ¹³⁴, K. Shigaki ⁸⁹, M. Shimomura ⁷⁵, Q. Shou ³⁹, S. Siddhanta ⁵¹, T. Siemiarczuk ⁷⁶, T.F. Silva ¹⁰⁶, W.D. Silva ¹⁰⁶, D. Silvermyr ⁷², T. Simantathammakul ¹⁰¹, R. Simeonov ³⁵, B. Singh ⁴⁶, B. Singh ⁸⁸, B. Singh ⁹², K. Singh ⁴⁷, R. Singh ⁷⁷, R. Singh ⁵³, S. Singh ¹⁵, T. Sinha ⁹⁶, B. Sitar ¹³, M. Sitta ^{130,55}, T.B. Skaali ¹⁹, G. Skorodumovs ⁹¹, N. Smirnov ¹³⁵, K.L. Smith ¹⁶, R.J.M. Snellings ⁵⁸, E.H. Solheim ¹⁹, S. Solokhin ⁸¹, C. Sonnabend ^{32,94}, J.M. Sonneveld ⁸¹, F. Soramel ²⁷, A.B. Soto-Hernandez ⁸⁵, R. Spijkers ⁸¹, C. Sporleder ¹¹³, I. Sputowska ¹⁰³, J. Staa ⁷², J. Stachel ⁹¹, L.L. Stahl ¹⁰⁶, I. Stan ⁶², A.G. Stejskal ¹¹⁴, T. Stellhorn ¹²³, S.F. Stiefelmaier ⁹¹, D. Stocco ⁹⁹, I. Storehaug ¹⁹, N.J. Strangmann ⁶³, P. Stratmann ¹²³, S. Strazzi ²⁵, A. Sturmiolo ^{115,30,52}, Y. Su ⁶, A.A.P. Suaide ¹⁰⁶, C. Suire ¹²⁸, A. Suiu ¹⁰⁹, M. Sukhanov ¹³⁹, M. Suljic ³², V. Sumberia ⁸⁸, S. Sumowidagdo ⁷⁹, P. Sun ¹⁰, N.B. Sundstrom ⁵⁸, L.H. Tabares ⁷, A. Tabikh ⁷⁰, S.F. Taghavi ⁹², J. Takahashi ¹⁰⁷, M.A. Talamantes Johnson ⁴³, G.J. Tambave ⁷⁷, Z. Tang ¹¹⁶, J. Tanwar ⁸⁷, J.D. Tapia Takaki ¹¹⁴, N. Tapus ¹⁰⁹, L.A. Tarasovicova ³⁶, M.G. Tarzila ⁴⁴, A. Tauro ³², A. Tavira García ^{104,128}, G. Tejeda Muñoz ⁴³, L. Terlizzi ²⁴, C. Terrevoli ⁴⁹, D. Thakur ⁵⁵, S. Thakur ⁴, M. Thogersen ¹⁹, D. Thomas ¹⁰⁴, A.M. Tieckötter ¹²³, N. Tiltmann ^{32,123}, A.R. Timmins ¹¹², A. Toia ⁶³, R. Tokumoto ⁸⁹, S. Tomassini ²⁵, K. Tomohiro ⁸⁹, Q. Tong ⁶, V.V. Torres ⁹⁹, A. Trifiró ^{30,52}, T. Triloki ⁹³, A.S. Triolo ³², S. Tripathy ³², T. Tripathy ¹²⁴, S. Trogolo ²⁴, V. Trubnikov ³, W.H. Trzaska ¹¹³, T.P. Trzcinski ¹³³, C. Tzolanta ¹⁹, R. Tu ³⁹, R. Turrisi ⁵³, T.S. Tveter ¹⁹, K. Ullaland ²⁰, B. Ulukutlu ⁹², S. Upadhyaya ¹⁰³, A. Uras ¹²⁵, M. Urioni ²³, G.L. Usai ²², M. Vaid ⁸⁸, M. Vala ³⁶, N. Valle ⁵⁴, L.V.R. van Doremalen ⁵⁸, M. van Leeuwen ⁸¹, C.A. van Veen ⁹¹, R.J.G. van Weelden ⁸¹, D. Varga ⁴⁵, Z. Varga ¹³⁵, P. Vargas Torres ⁶⁴, O. Vázquez Doce ⁴⁸, O. Vazquez Rueda ¹¹², G. Vecil ²³, P. Veen ¹²⁷, E. Vercellin ²⁴, R. Verma ⁴⁶, R. Vértési ⁴⁵, M. Verweij ⁵⁸, L. Vickovic ³³, Z. Vilakazi ¹²⁰, A. Villani ²³, C.J.D. Villiers ⁶⁷, T. Virgili ²⁸, M.M.O. Virta ⁴², A. Vodopyanov ¹³⁹, M.A. Völkl ⁹⁷, S.A. Voloshin ¹³⁴, G. Volpe ³¹, B. von Haller ³², I. Vorobyev ³², N. Vozniuk ¹³⁹, J. Vrláková ³⁶, J. Wan ³⁹, C. Wang ³⁹, D. Wang ³⁹, Y. Wang ¹¹⁶, Y. Wang ³⁹, Y. Wang ⁶, Z. Wang ³⁹, F. Weiglhofer ³², S.C. Wenzel ³², J.P. Wessels ¹²³, P.K. Wiacek ², J. Wiechula ⁶³, J. Wikne ¹⁹, G. Wilk ⁷⁶, J. Wilkinson ⁹⁴, G.A. Willems ¹²³, N. Wilson ¹¹⁵, B. Windelband ⁹¹, J. Witte ⁹¹, M. Wojnar ², C.I. Worek ², J.R. Wright ¹⁰⁴, C.-T. Wu ^{6,27}, W. Wu ^{92,39}, Y. Wu ¹¹⁶, K. Xiong ³⁹, Z. Xiong ¹¹⁶, L. Xu ^{125,6}, R. Xu ⁶, Z. Xue ⁷¹, A. Yadav ⁴¹, A.K. Yadav ¹³², Y. Yamaguchi ⁸⁹, S. Yang ⁵⁷, S. Yang ²⁰, S. Yano ⁸⁹, Z. Ye ⁷¹, E.R. Yeats ¹⁸, J. Yi ⁶, R. Yin ³⁹, Z. Yin ⁶, I.-K. Yoo ¹⁶, J.H. Yoon ⁵⁷, H. Yu ¹², S. Yuan ²⁰, A. Yuncu ⁹¹, V. Zaccolo ²³, C. Zampolli ³², F. Zanone ⁹¹, N. Zardoshti ³², P. Závada ⁶¹, B. Zhang ⁹¹, C. Zhang ¹²⁷, L. Zhang ³⁹, M. Zhang ^{124,6}, M. Zhang ^{27,6}, S. Zhang ³⁹, X. Zhang ⁶, Y. Zhang ¹¹⁶, Y. Zhang ¹¹⁶, Z. Zhang ⁶, D. Zhou ⁶, Y. Zhou ⁸⁰, Z. Zhou ³⁹, J. Zhu ³⁹, S. Zhu ^{94,116}, Y. Zhu ⁶, A. Zingaretti ²⁷, S.C. Zugravel ⁵⁵, N. Zurlo ^{131,54}

Affiliation Notes

¹ Deceased

- ^{II} Also at: Max-Planck-Institut für Physik, Munich, Germany
- ^{III} Also at: Czech Technical University in Prague (CZ)
- ^{IV} Also at: Instituto de Física da Universidade de São Paulo
- ^V Also at: Dipartimento DET del Politecnico di Torino, Turin, Italy
- ^{VI} Also at: Department of Applied Physics, Aligarh Muslim University, Aligarh, India
- ^{VII} Also at: Institute of Theoretical Physics, University of Wrocław, Poland
- ^{VIII} Also at: Facultad de Ciencias, Universidad Nacional Autónoma de México, Mexico City, Mexico

Collaboration Institutes

- ¹ A.I. Alikhanyan National Science Laboratory (Yerevan Physics Institute) Foundation, Yerevan, Armenia
- ² AGH University of Krakow, Cracow, Poland
- ³ Bogolyubov Institute for Theoretical Physics, National Academy of Sciences of Ukraine, Kyiv, Ukraine
- ⁴ Bose Institute, Department of Physics and Centre for Astroparticle Physics and Space Science (CAPSS), Kolkata, India
- ⁵ California Polytechnic State University, San Luis Obispo, California, United States
- ⁶ Central China Normal University, Wuhan, China
- ⁷ Centro de Aplicaciones Tecnológicas y Desarrollo Nuclear (CEADEN), Havana, Cuba
- ⁸ Centro de Investigación y de Estudios Avanzados (CINVESTAV), Mexico City and Mérida, Mexico
- ⁹ Chicago State University, Chicago, Illinois, United States
- ¹⁰ China Nuclear Data Center, China Institute of Atomic Energy, Beijing, China
- ¹¹ China University of Geosciences, Wuhan, China
- ¹² Chungbuk National University, Cheongju, Republic of Korea
- ¹³ Comenius University Bratislava, Faculty of Mathematics, Physics and Informatics, Bratislava, Slovak Republic
- ¹⁴ Creighton University, Omaha, Nebraska, United States
- ¹⁵ Department of Physics, Aligarh Muslim University, Aligarh, India
- ¹⁶ Department of Physics, Pusan National University, Pusan, Republic of Korea
- ¹⁷ Department of Physics, Sejong University, Seoul, Republic of Korea
- ¹⁸ Department of Physics, University of California, Berkeley, California, United States
- ¹⁹ Department of Physics, University of Oslo, Oslo, Norway
- ²⁰ Department of Physics and Technology, University of Bergen, Bergen, Norway
- ²¹ Dipartimento di Fisica, Università di Pavia, Pavia, Italy
- ²² Dipartimento di Fisica dell'Università and Sezione INFN, Cagliari, Italy
- ²³ Dipartimento di Fisica dell'Università and Sezione INFN, Trieste, Italy
- ²⁴ Dipartimento di Fisica dell'Università and Sezione INFN, Turin, Italy
- ²⁵ Dipartimento di Fisica e Astronomia dell'Università and Sezione INFN, Bologna, Italy
- ²⁶ Dipartimento di Fisica e Astronomia dell'Università and Sezione INFN, Catania, Italy
- ²⁷ Dipartimento di Fisica e Astronomia dell'Università and Sezione INFN, Padova, Italy
- ²⁸ Dipartimento di Fisica 'E.R. Caianiello' dell'Università and Gruppo Collegato INFN, Salerno, Italy
- ²⁹ Dipartimento DISAT del Politecnico and Sezione INFN, Turin, Italy
- ³⁰ Dipartimento di Scienze MIFT, Università di Messina, Messina, Italy
- ³¹ Dipartimento Interateneo di Fisica 'M. Merlin' and Sezione INFN, Bari, Italy
- ³² European Organization for Nuclear Research (CERN), Geneva, Switzerland
- ³³ Faculty of Electrical Engineering, Mechanical Engineering and Naval Architecture, University of Split, Split, Croatia
- ³⁴ Faculty of Nuclear Sciences and Physical Engineering, Czech Technical University in Prague, Prague, Czech Republic
- ³⁵ Faculty of Physics, Sofia University, Sofia, Bulgaria
- ³⁶ Faculty of Science, P.J. Šafárik University, Košice, Slovak Republic
- ³⁷ Faculty of Technology, Environmental and Social Sciences, Bergen, Norway
- ³⁸ Frankfurt Institute for Advanced Studies, Johann Wolfgang Goethe-Universität Frankfurt, Frankfurt, Germany
- ³⁹ Fudan University, Shanghai, China
- ⁴⁰ Gauhati University, Department of Physics, Guwahati, India
- ⁴¹ Helmholtz-Institut für Strahlen- und Kernphysik, Rheinische Friedrich-Wilhelms-Universität Bonn, Bonn, Germany
- ⁴² Helsinki Institute of Physics (HIP), Helsinki, Finland

- 43 High Energy Physics Group, Universidad Autónoma de Puebla, Puebla, Mexico
- 44 Horia Hulubei National Institute of Physics and Nuclear Engineering, Bucharest, Romania
- 45 HUN-REN Wigner Research Centre for Physics, Budapest, Hungary
- 46 Indian Institute of Technology Bombay (IIT), Mumbai, India
- 47 Indian Institute of Technology Indore, Indore, India
- 48 INFN, Laboratori Nazionali di Frascati, Frascati, Italy
- 49 INFN, Sezione di Bari, Bari, Italy
- 50 INFN, Sezione di Bologna, Bologna, Italy
- 51 INFN, Sezione di Cagliari, Cagliari, Italy
- 52 INFN, Sezione di Catania, Catania, Italy
- 53 INFN, Sezione di Padova, Padova, Italy
- 54 INFN, Sezione di Pavia, Pavia, Italy
- 55 INFN, Sezione di Torino, Turin, Italy
- 56 INFN, Sezione di Trieste, Trieste, Italy
- 57 Inha University, Incheon, Republic of Korea
- 58 Institute for Gravitational and Subatomic Physics (GRASP), Utrecht University/Nikhef, Utrecht, Netherlands
- 59 Institute of Experimental Physics, Slovak Academy of Sciences, Košice, Slovak Republic
- 60 Institute of Physics, Homi Bhabha National Institute, Bhubaneswar, India
- 61 Institute of Physics of the Czech Academy of Sciences, Prague, Czech Republic
- 62 Institute of Space Science (ISS), Bucharest, Romania
- 63 Institut für Kernphysik, Johann Wolfgang Goethe-Universität Frankfurt, Frankfurt, Germany
- 64 Instituto de Ciencias Nucleares, Universidad Nacional Autónoma de México, Mexico City, Mexico
- 65 Instituto de Física, Universidade Federal do Rio Grande do Sul (UFRGS), Porto Alegre, Brazil
- 66 Instituto de Física, Universidad Nacional Autónoma de México, Mexico City, Mexico
- 67 iThemba LABS, National Research Foundation, Somerset West, South Africa
- 68 Jeonbuk National University, Jeonju, Republic of Korea
- 69 Korea Institute of Science and Technology Information, Daejeon, Republic of Korea
- 70 Laboratoire de Physique Subatomique et de Cosmologie, Université Grenoble-Alpes, CNRS-IN2P3, Grenoble, France
- 71 Lawrence Berkeley National Laboratory, Berkeley, California, United States
- 72 Lund University Department of Physics, Division of Particle Physics, Lund, Sweden
- 73 Marietta Blau Institute, Vienna, Austria
- 74 Nagasaki Institute of Applied Science, Nagasaki, Japan
- 75 Nara Women's University (NWU), Nara, Japan
- 76 National Centre for Nuclear Research, Warsaw, Poland
- 77 National Institute of Science Education and Research, Homi Bhabha National Institute, Jatni, India
- 78 National Nuclear Research Center, Baku, Azerbaijan
- 79 National Research and Innovation Agency - BRIN, Jakarta, Indonesia
- 80 Niels Bohr Institute, University of Copenhagen, Copenhagen, Denmark
- 81 Nikhef, National institute for subatomic physics, Amsterdam, Netherlands
- 82 Nuclear Physics Group, STFC Daresbury Laboratory, Daresbury, United Kingdom
- 83 Nuclear Physics Institute of the Czech Academy of Sciences, Husinec-Řež, Czech Republic
- 84 Oak Ridge National Laboratory, Oak Ridge, Tennessee, United States
- 85 Ohio State University, Columbus, Ohio, United States
- 86 Physics department, Faculty of science, University of Zagreb, Zagreb, Croatia
- 87 Physics Department, Panjab University, Chandigarh, India
- 88 Physics Department, University of Jammu, Jammu, India
- 89 Physics Program and International Institute for Sustainability with Knotted Chiral Meta Matter (WPI-SKCM²), Hiroshima University, Hiroshima, Japan
- 90 Physikalisches Institut, Eberhard-Karls-Universität Tübingen, Tübingen, Germany
- 91 Physikalisches Institut, Ruprecht-Karls-Universität Heidelberg, Heidelberg, Germany
- 92 Physik Department, Technische Universität München, Munich, Germany
- 93 Politecnico di Bari and Sezione INFN, Bari, Italy
- 94 Research Division and ExtreMe Matter Institute EMMI, GSI Helmholtzzentrum für Schwerionenforschung GmbH, Darmstadt, Germany
- 95 Saga University, Saga, Japan

- ⁹⁶ Saha Institute of Nuclear Physics, Homi Bhabha National Institute, Kolkata, India
- ⁹⁷ School of Physics and Astronomy, University of Birmingham, Birmingham, United Kingdom
- ⁹⁸ Sección Física, Departamento de Ciencias, Pontificia Universidad Católica del Perú, Lima, Peru
- ⁹⁹ SUBATECH, IMT Atlantique, Nantes Université, CNRS-IN2P3, Nantes, France
- ¹⁰⁰ Sungkyunkwan University, Suwon City, Republic of Korea
- ¹⁰¹ Suranaree University of Technology, Nakhon Ratchasima, Thailand
- ¹⁰² Technical University of Košice, Košice, Slovak Republic
- ¹⁰³ The Henryk Niewodniczanski Institute of Nuclear Physics, Polish Academy of Sciences, Cracow, Poland
- ¹⁰⁴ The University of Texas at Austin, Austin, Texas, United States
- ¹⁰⁵ Universidad Autónoma de Sinaloa, Culiacán, Mexico
- ¹⁰⁶ Universidade de São Paulo (USP), São Paulo, Brazil
- ¹⁰⁷ Universidade Estadual de Campinas (UNICAMP), Campinas, Brazil
- ¹⁰⁸ Universidade Federal do ABC, Santo Andre, Brazil
- ¹⁰⁹ Universitatea Nationala de Stiinta si Tehnologie Politehnica Bucuresti, Bucharest, Romania
- ¹¹⁰ University of Cape Town, Cape Town, South Africa
- ¹¹¹ University of Derby, Derby, United Kingdom
- ¹¹² University of Houston, Houston, Texas, United States
- ¹¹³ University of Jyväskylä, Jyväskylä, Finland
- ¹¹⁴ University of Kansas, Lawrence, Kansas, United States
- ¹¹⁵ University of Liverpool, Liverpool, United Kingdom
- ¹¹⁶ University of Science and Technology of China, Hefei, China
- ¹¹⁷ University of Silesia in Katowice, Katowice, Poland
- ¹¹⁸ University of South-Eastern Norway, Kongsberg, Norway
- ¹¹⁹ University of Tennessee, Knoxville, Tennessee, United States
- ¹²⁰ University of the Witwatersrand, Johannesburg, South Africa
- ¹²¹ University of Tokyo, Tokyo, Japan
- ¹²² University of Tsukuba, Tsukuba, Japan
- ¹²³ Universität Münster, Institut für Kernphysik, Münster, Germany
- ¹²⁴ Université Clermont Auvergne, CNRS/IN2P3, LPC, Clermont-Ferrand, France
- ¹²⁵ Université de Lyon, CNRS/IN2P3, Institut de Physique des 2 Infinis de Lyon, Lyon, France
- ¹²⁶ Université de Strasbourg, CNRS, IPHC UMR 7178, F-67000 Strasbourg, France, Strasbourg, France
- ¹²⁷ Université Paris-Saclay, Centre d'Etudes de Saclay (CEA), IRFU, Département de Physique Nucléaire (DPhN), Saclay, France
- ¹²⁸ Université Paris-Saclay, CNRS/IN2P3, IJCLab, Orsay, France
- ¹²⁹ Università degli Studi di Foggia, Foggia, Italy
- ¹³⁰ Università del Piemonte Orientale, Vercelli, Italy
- ¹³¹ Università di Brescia, Brescia, Italy
- ¹³² Variable Energy Cyclotron Centre, Homi Bhabha National Institute, Kolkata, India
- ¹³³ Warsaw University of Technology, Warsaw, Poland
- ¹³⁴ Wayne State University, Detroit, Michigan, United States
- ¹³⁵ Yale University, New Haven, Connecticut, United States
- ¹³⁶ Yildiz Technical University, Istanbul, Turkey
- ¹³⁷ Yonsei University, Seoul, Republic of Korea
- ¹³⁸ Affiliated with an institute formerly covered by a cooperation agreement with CERN
- ¹³⁹ Affiliated with an international laboratory covered by a cooperation agreement with CERN.